


Carboniferous tectono-magmatic evolution of the northern Luliang arc: evidence from geochemistry and petrography of Carboniferous volcanic rocks in the northern Luliang Uplift, NW China

Sijie Han¹  · Shuxun Sang^{1,2,3} · Wenfeng Wang^{2,3} · Jinchao Zhang^{2,3} · Guanlong Zhang⁴

Received: 5 November 2020 / Revised: 23 December 2020 / Accepted: 4 February 2021 / Published online: 26 February 2021
© Science Press and Institute of Geochemistry, CAS and Springer-Verlag GmbH Germany, part of Springer Nature 2021

Abstract The Northern Junggar Basin experienced extensive subduction and a complex tectono-magmatic evolution during the Late Paleozoic, resulting in a heterogeneous distribution of volcanic rocks in the Junggar Basin. In this study, the Carboniferous tectono-magmatic evolution of the northern Luliang arc was described by exploring the petrography and geochemistry of Carboniferous volcanic rocks collected from well Y-2 and outcrop WW' in the northern Luliang Uplift. The distribution, types, and formation ages of these volcanic rocks were characterized and the volcanic sequence in well Y-1 was divided into upper and lower parts according to vertical variations in selected geochemical data. Then the petrogenesis and tectonic settings of different volcanic rocks were evaluated and this was used to infer the tectono-magmatic evolution of the northern Luliang arc during the Carboniferous. The results indicate that: (1) Carboniferous high-K calc-alkali andesite–dacite associations are distributed in the west of the northern Luliang Uplift, and Lower Carboniferous calc-alkali basalt–dacite–rhyolite assemblages are preserved in its east. (2) The intermediate-

acid volcanic rocks in wells Y-1 and Y-2 were derived from calc-alkali basaltic magma through melting of the juvenile lower crust, and geochemical variations indicate increasing addition of slab melting in a subduction-related arc environment. The bimodal volcanic rocks from outcrop WW' were derived from lithospheric underplating of basaltic magma in an intra-arc extensional setting. (3) The closure of the eastern Keramaili Oceanic basin occurred before the Early Carboniferous, and the tectono-magmatic difference between the east and the west of the northern Luliang Uplift appeared before the Carboniferous period.

Keywords Tectonic setting · Bimodal volcanic rocks · Carboniferous · Keramaili oceanic basin · Subduction · Northern Luliang arc

1 Introduction

The Junggar Basin and its surrounding areas experienced a complex tectonic evolution and sedimentary filling due to the closure of the Junggar Oceanic basin, which resulted in the production of a variety of tectonic settings, including oceanic island arcs, continental arcs, within-plate rifts, and post-collisional extensional environment (Han et al. 2015; Li et al. 2015a, b; Wu et al. 2009; Su et al. 2011). Several scholars have reported on the petrology, geochemistry, geochronology, and geophysical properties of the Carboniferous volcano-related rock associations from different areas within the Junggar Basin (Kou et al. 2010; Xiao et al. 2011; Yang et al. 2014b); moreover, various mantle source signatures and tectonic transitions have been recorded for these volcanic rocks (Liang et al. 2017; Su et al. 2012; Zhang et al. 2016). Significant variations of petrography and geochemistry exist in the Carboniferous volcanic

✉ Sijie Han
hsj_cumt@126.com

¹ Low Carbon Energy Research Institute, China University of Mining and Technology, Xuzhou 221008, China

² Key Laboratory of Coalbed Methane Resources and Reservoir Formation Process of the Ministry of Education, China University of Mining and Technology, Xuzhou 221008, China

³ School of Resource and Earth Sciences, China University of Mining and Technology, Xuzhou 221116, China

⁴ Research Institute of Petroleum Exploration and Development, Shengli Oilfield Company, Dongying 257000, China

rocks, and those rocks in the Luliang Uplift may have different petrogenesis (Tan et al. 2009; Wu et al. 2011; Zhang et al. 2015a, b). Multiple subductions of different oceanic basins (e.g., the Keramaili Oceanic basin and the Junggar Oceanic basin) occurred around the Luliang arc (the Luliang Uplift was called Luliang arc during the Late Paleozoic) during the Carboniferous; therefore, the Carboniferous volcanic rocks in various areas also have different petrographic and geochemical characteristics. As a result, previous studies have suggested that different petrogenetic and tectonic settings including an arc environment (Zhang et al. 2008b, 2018), oceanic ridge subduction (Geng et al. 2009, 2011), an intra-oceanic arc (Shen et al. 2013), and a rift setting (Wang et al. 2002) existed concurrently in the Luliang arc during the Carboniferous.

Tectonically, the Luliang Uplift has been broadly characterized as having an “uplift–graben–uplift” profile from north to south (Yang et al. 2004), and the Carboniferous volcanic rocks have been shown to have an anisotropic compositional distribution (Zhou et al. 2018). There has been much controversy over the tectonic setting and the evolution of the Luliang arc as indicated by the nature of these volcanic rocks. Uplift-type mafic rocks, mainly preserved in the eastern parts of the Luliang Uplift indicate a post-collisional extensional environment, and these high-K calc-alkali basalts show a wide range of eruption ages from 350 ± 6.3 to 308.6 ± 4.7 Ma (Tan et al. 2009; Yang et al. 2010; Li et al. 2015a; Luo et al. 2017). The Lower Carboniferous rhyolitic tuffs in well DX-14 of the eastern part of the Luliang Uplift conversely show some crust-derived characteristics, indicating a continental active arc environment (Li et al. 2012). Compared to the volcano-related rocks in the eastern part of the Luliang Uplift, significantly different rock associations in the western parts of the Luliang Uplift indicate the difference in their geodynamics as well. Ocean island basalt (OIB)-like alkaline and calc-alkaline volcanic rocks (basalt–andesite–dacite assemblages) have been identified in the western parts of the Luliang Uplift and have been interpreted as being derived from the upwelling of an asthenospheric mantle through a slab window during ridge subduction (Geng et al. 2009; Yang et al. 2016). Conversely, the Carboniferous volcanic rocks in the southern, central, and western parts of the Luliang Uplift are significantly associated with arc-volcanic rocks derived from the thickened crust of a mature arc environment (Zhang et al. 2008a; Li et al. 2015b). Recently, Zhang et al. (2018) reported arc-type calc-alkali volcanic rocks yielding a Ziron LA-ICP-MS age of 310.8 ± 2.9 Ma in the western parts of the Luliang Uplift, clearly indicating a subduction-related continental arc setting, which is in good agreement with the previous investigation (Han et al. 2019b). However, previous studies have mainly focused on the results of subduction of the Junggar

Oceanic basin in the southern parts of the Luliang arc (Long et al. 2006; Li et al. 2014; Xu et al. 2015; Zheng et al. 2019), and few studies focused on the Carboniferous volcanic rocks that have been derived from the subduction of the Keramaili Oceanic basin. This may be attributed to the following reasons: (1) the volcanic rocks are less accessible, and (2) bidirectional subduction of the Keramaili Oceanic basin has been neglected due to a lack of comprehensive investigations. The closure age of the Keramaili Oceanic basin is thus not well understood, and nor are the different tectono-magmatic evolutionary histories between the eastern and the western parts of the northern Luliang arc during the Carboniferous.

In this study, new volcanic rock samples of the northern Luliang Uplift (seven from the eastern and two from the western part of the northern Luliang Uplift) were collected and studied, and these results together with the published data were used to investigate the petrogenesis and tectonic setting. First, the spatial and temporal distribution of the Carboniferous volcanic rocks of the northern Luliang Uplift were studied and volcanic rock formation age constraints for well Y-1 were obtained. Furthermore, selected geochemical indicators were then used to discern a geochemical transition within well Y-1, and the reason for its occurrence was explored. Third, the petrogenesis of these volcanic rocks, which range from mafic to felsic rock associations, was discussed. Finally, geochemical results and other geological evidence obtained in this study were applied to interpret the tectono-magmatic evolution of the northern margin of the Luliang arc during the Carboniferous. This study aimed to comprehensively explore the geodynamic differences across the northern Luliang arc during the Carboniferous and to accurately specify the differences in the tectono-magmatic evolution resulting from the subduction of the Keramaili Oceanic basin.

2 Geological setting

The Junggar Basin is located at the southern margin of the Central Asian Orogenic Belt and lies at the junction between Siberia, Russia, and the Tarim Plate (Fig. 1a). Late Paleozoic ophiolitic mélangé, granitoids, and subduction-related volcanic rocks widely occur in suture orogenic belts around the Junggar Basin (Fig. 1b, e.g. Windley et al. 2007; Chen et al. 2010; Tang et al. 2010), indicating multiple subductions of oceanic crust and microplate collisions. Tectonically, the Junggar Basin is composed of the Wulungu Depression, the Luliang Uplift, the West Uplift, the Central Depression, the East Uplift, and the North Tianshan Thrust Belt. The tectonic framework of the Luliang Uplift after post-Carboniferous tectonic movements has been characterized as “uplift–graben–uplift”

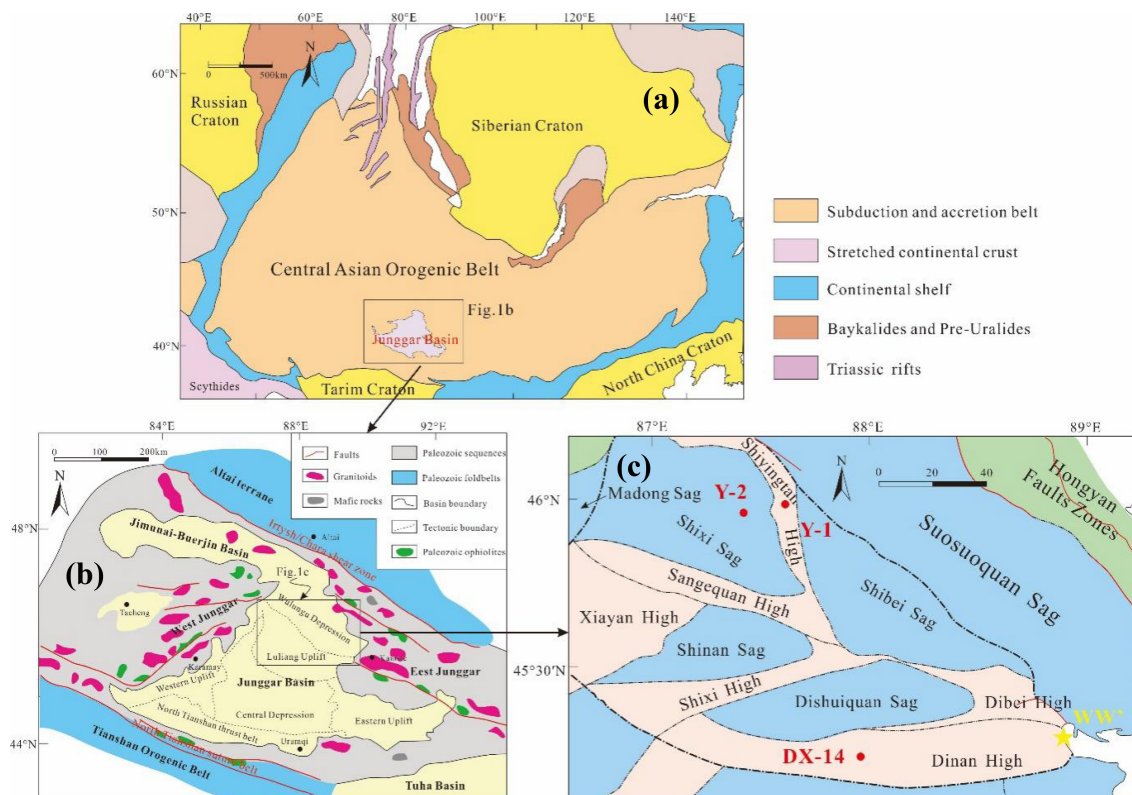


Fig. 1 **a** Location of the study area in the Central Asian Orogenic Belt (Şengör et al. 2018); **b** Simplified geological map of the Junggar basin and surrounding areas (Li et al. 2015b); **c** The locations of wells Y-1, Y-2 and DX-14 and outcrop WW' in the northern Luliang Uplift (Li et al. 2012; Han et al. 2019b)

from south to north (Yang et al. 2004). The Shiyintan high and the Dibe high are the secondary tectonic units, located in the western and the eastern parts of the northern Luliang Uplift. The northern part of the Luliang Uplift is sutured to the Wulungu Depression and records the southward subduction of the Keramaili Oceanic basin. Wells Y-1 and Y-2 are located in the western area, and outcrop WW' lies in the eastern area, as shown in Fig. 1c.

What is now termed as the Luliang Uplift was denoted as the Luliang arc in the Late Paleozoic. This arc formed due to the northward subduction of the Junggar Ocean during the Carboniferous. Significant subduction in the Devonian resulted in the emplacement of a large volume of arc-volcanic rock, and the Early Carboniferous tectonic framework was inherited from that of the Devonian. However, from the middle of the Carboniferous, a dramatic change occurred in the tectono-sedimentary environment, and thus different types of volcano-related rocks were emplaced in the eastern and the western parts of the Luliang arc (Yang et al. 2012). The tectonic differences indicated by this spatial variability have been attributed to the scissor-like closure of the Keramaili Ocean (Li et al. 2012; Han et al. 2019a). Furthermore, previous studies have suggested that, though there is still controversy over the related tectonic setting, the basalt–andesite–dacite

associations in the western Luliang arc can be interpreted as arc-like (Zhang et al. 2008a, 2018; Geng et al. 2011). Conversely, investigations of mafic rocks in the eastern Luliang arc and the East Junggar area have concluded that their emplacement resulted from the roll-back of the subducted crust of the Junggar Ocean, which caused extension in the Luliang arc and formation of an intra-arc extensional basin (Su et al. 2012; Li et al. 2015a). During the end of the Late Carboniferous to the Middle Permian, the eastern Luliang Uplift was transformed into a continental magmatic arc system (Xiao et al. 2009), and the tectonic evolution of the basin entered an intra-continental stage. At this time, the Luliang arc experienced significant uplift and denudation, resulting in the incomplete preservation of the Carboniferous stratigraphy (Li et al. 2015a).

Boreholes and geophysical results have revealed that Mesozoic–Cenozoic sedimentary rocks directly covered the underlying Carboniferous volcanic rock basement in the Luliang Uplift (Yang et al. 2014a; Tao et al. 2013). However, these Carboniferous volcanic rocks present significant heterogeneity in their distribution and composition. This may be attributed to the following two reasons: 1) subduction was of the Keramaili Ocean and Junggar Ocean, respectively, to the north and the south of the Luliang arc during the Late Paleozoic (Li et al. 2016), and

2) non-synchronous closure of the Keramaili Ocean contributed to diachronous volcano-sedimentary sequences during the Late Carboniferous (Han et al. 2019b). The Lower Carboniferous volcanic sequences, consisting of intermediate volcanic rocks and related pyroclastic rocks, are widely distributed in the Luliang Uplift. Moreover, some post-collisional basalts with characteristics inherited from arc volcanic rocks occur in the eastern Luliang Uplift (Su et al. 2010). The volume of the bimodal volcanic rocks exhibits an eastwardly increasing trend extending into the East Junggar terrane (Su et al. 2012). The Upper Carboniferous volcanic sequences are only exposed in the eastern Luliang Uplift and Shiyintan area, and a significant difference is observed in the rock associations and their compositions in these two areas compared to rocks from the Lower Carboniferous.

3 Samples and analytical methods

Seven volcanic rocks from outcrop WW' and two dacite samples from well Y-2 were collected to better understand the dynamic setting in the northern Luliang arc during the Carboniferous. Moreover, whole-rock geochemical data that are available for all 12 volcanic rocks with low loss of ignition (LOI) in well Y-1 were also considered (Han et al. 2019b). Data for samples WW'8 (basalt) reported in our previous publication are also referenced (Han et al. 2015). Before the geochemical analysis, petrographic observations under plane-polarized and cross-polarized light were carried out to select fresh samples.

Major elements and some trace elements (except for U, Cs, Ta, Sn, and rare earth elements (REEs)) were detected by X-ray fluorescence (XRF, BRUKER S8 TIGER) spectroscopy, with standard deviations within 2%. The concentrations of U, Cs, Sn, Ta, and REEs were obtained by inductively coupled plasma mass spectrometry (ICP-MS) using an X Series-2 spectrometer. The detailed procedures for determining the concentrations of major and trace elements are reported by Gou et al. (2013). The limits of detection for the major and some trace elements (except for U, Cs, Sn, Ta, and REEs) were 0.1% and 1 ppm, respectively. The lowest detection limit for U, Cs, Ta, Sn, and REE was about 0.1 ppm. Furthermore, the USGS standard AGV-1 and the Chinese national rock standard GSR-2 were used as standard reference materials during the analysis to monitor the accuracy of the data (Cheng et al. 2015; Gladney et al. 1992). The whole-rock geochemical data for these 22 samples are presented in Table 1.

4 Petrography

In general, the volcanic rocks exposed at outcrop WW' exhibit a typical bimodal nature, with rhyolite/dacite occurring initially and significant basalt/basaltic andesite arising later. Their length ratio in the section is approximately 1:4, indicating that mafic rocks dominate rock associations in the east of the northern Luliang Uplift. Andesite, dacite, and minor tuff are found within wells Y-1 and Y-2. Moreover, some basaltic andesites occurred in the upper volcanic sequence of well Y-1, and quartz and alkali feldspar occurred widely in the lower volcanic sequence of well Y-1.

The basalts display a porphyritic texture, with plagioclase (up to 65%) and pyroxene phenocrysts set in a groundmass of plagioclase, clinopyroxene, and minor Fe–Ti oxides (Fig. 2a). The plagioclases are subhedral and their sizes range from 0.1 to 0.5 mm, and the pyroxenes are subhedral–euhedral, averaging 0.5 mm in size. The crystal size distributions in the porphyritic lavas and the enrichment in plagioclase relative to pyroxene indicate the accumulation of plagioclase in the magma. The fine-grained rhyolite is made up of alkali feldspar (up to 0.4 mm), quartz (0.05 mm), and plagioclase, with minor amounts of hornblende and biotite (Fig. 2b).

The andesite shows a porphyritic texture, and its phenocrysts consist of plagioclase (up to 0.5 mm), pyroxene (0.2 mm), and hornblende (0.2 mm) (Fig. 2c, d). The plagioclases are slabby or columnar, commonly with corroded margins. In contrast, the pyroxenes form octagonal graininess and consist of two groups of near orthometric cleavage planes. The hornblendes show a rhombic section and darkened margins. The matrix, made up of 0.02 mm crystals, presents a hyalopilitic texture, and the microcrystals are needle-like plagioclase and strip-like hornblende containing minor crypto-crystalline or glassy components. The basaltic andesites are aphyric, and the matrix mainly consists of the 0.2-mm-long strip- and needle-shaped plagioclase (Fig. 2e). Granular pyroxenes, characterized by some chloritization, fill the voids between the plagioclase crystals.

Figure 2f exhibits that the phenocrysts in the dacite include columnar plagioclase, slabby alkali feldspar, and columnar hornblende with an average size of 0.2 mm. Fine-grained hornblendes are trapped in alkali-feldspar phenocrysts. The matrix is mainly needle-like microcrystalline plagioclase (0.02 mm) showing a pilotaxitic texture.

Crystal pyroclasts account for 50%–60% of the tuff, which contains orthoclase, quartz, plagioclase, and hornblende pyroclasts. Figure 2g shows that the rhombic orthoclase and angular to sub-rounded quartz are the main

Table 1 Major element (wt.%) and trace elements (ppm) analyses of Carboniferous volcanic rocks from field profile WW' and well Y-1 and Y-2. The data from Y-1 are cited from Han et al. (2019b), Samples WW'-8 was also cited from our previous published paper (Han et al. 2015)

Samples	WW'1	WW'2	WW'3	WW'4	WW'5	WW'6	WW'7	WW'8	Y2-1	Y2-2	Y1-3
Depth/m	30	280	672	676	1077	1596	1796	2016	3525	3880	2634
Lithology	Rhyolite	Rhyolite	Rhyolite	Dacite	Basalt	Basalt	Basalt	Basalt	Dacite	Dacite	Andesite
SiO ₂	69.09	68.89	75.52	64.69	53.97	50.24	52.07	52.85	65.23	63.61	58.76
Na ₂ O	4.35	6.67	3.27	5.04	6.18	3.54	4.46	6.72	4.11	3.92	2.32
K ₂ O	3.55	1.08	4.65	2.76	0.39	1.28	0.93	1.55	2.68	2.99	1.9
Al ₂ O ₃	12.84	12.72	12.03	15.16	17.21	16.74	17.12	15.00	14.82	15.25	18.72
TFe ₂ O ₃	4.90	4.60	1.67	4.56	8.53	10.40	9.98	11.21	5.56	4.46	8.15
CaO	1.02	2.99	0.36	2.79	6.54	7.06	8.36	5.76	4.93	4.16	2.68
MgO	0.53	0.52	0.30	0.98	2.50	4.19	3.99	3.27	1.37	2.30	1.81
TiO ₂	0.31	0.34	0.12	0.77	1.50	1.74	1.68	2.63	0.70	0.59	1.00
P ₂ O ₅	0.05	0.07	0.03	0.31	0.51	0.47	0.57	0.83	0.18	0.18	0.13
MnO	0.23	0.16	0.04	0.14	0.16	0.16	0.12	0.36	0.07	0.09	0.10
LOI	3.11	2.01	1.94	3.12	3.25	4.97	1.56	1.21	0.42	2.50	4.61
Total	99.99	100.06	99.93	100.32	100.73	100.79	100.83	101.40	100.06	100.04	100.18
Sc	18.90	25.90	6.70	9.10	27.10	29.00	27.90	29.20	13.80	10.90	19.6
V	17.20	16.40	7.00	41.80	202.40	225.00	223.50	183.00	109.50	99.10	148
Cr	13.30	7.40	nd	nd	135.30	108.90	123.30	33.00	213.70	149.20	257.2
Co	26.80	18.20	19.80	16.00	34.40	27.30	48.90	21.40	12.60	13.30	18
Ni	28.60	19.30	22.50	14.70	76.70	27.10	83.10	nd	24.40	17.30	49.1
Cu	13.60	11.20	5.00	5.60	32.50	39.70	45.30	19.40	68.30	53.40	85.4
Zn	106.60	121.10	45.10	74.60	116.10	87.20	83.10	158.30	77.40	69.10	158
Ga	23.40	27.10	12.40	20.50	18.90	19.70	20.20	24.90	17.20	17.40	22.9
Rb	82.10	25.80	118.10	74.70	5.80	38.70	10.50	25.40	72.20	83.90	58.4
Sr	51.40	51.00	65.20	191.10	587.20	350.90	497.10	372.50	287.40	382.00	143.1
Zr	215.90	227.20	189.80	164.90	151.20	135.30	173.90	190.20	111.70	145.60	201.5
Nb	46.10	37.10	22.30	41.80	19.10	19.60	8.90	42.90	15.20	6.40	11.9
Ba	847.80	388.30	475.80	921.70	292.60	240.30	251.10	360.70	1771.00	1608.20	431.2
Hf	12.50	11.30	7.20	9.40	5.40	5.30	5.10	10.20	4.60	4.40	6.1
Pb	15.00	15.90	16.50	17.20	7.10	6.60	4.20	11.60	13.40	9.60	ab
Th	14.70	9.40	8.70	13.00	nd	8.60	nd	12.10	8.10	5.00	8.2
Sn	3.49	2.76	3.09	3.34	2.46	6.35	1.53	0.95	15.56	2.51	49.91
Cs	1.57	2.32	5.10	3.01	1.41	2.24	0.35	0.90	1.83	1.19	3.50
Ta	2.41	1.90	2.21	1.45	0.70	1.08	1.04	1.42	0.41	0.39	0.64
U	2.27	2.18	2.30	1.28	0.81	0.64	0.45	1.24	1.82	1.78	1.72
Y	50.65	52.67	43.11	30.62	29.59	28.53	29.25	35.50	14.11	15.05	27.15
La	24.04	28.40	31.16	22.21	23.00	15.78	21.90	28.46	16.49	17.92	22.81
Ce	53.94	69.24	63.66	50.67	45.21	37.82	48.90	60.52	33.39	36.72	46.63
Pr	7.78	8.77	8.73	6.82	7.08	5.59	6.77	8.18	4.46	4.86	5.73
Nd	32.60	36.76	32.32	27.72	29.97	25.09	28.50	33.95	18.43	19.85	23.52
Sm	7.68	8.43	6.95	5.84	6.48	5.79	6.08	7.17	3.73	3.98	5.08
Eu	1.90	2.24	0.61	1.42	1.88	1.92	1.83	2.00	1.00	1.03	1.29
Gd	7.24	7.77	6.27	5.24	5.69	5.17	5.59	6.49	3.28	3.38	4.88
Tb	1.49	1.55	1.26	0.97	1.04	0.97	1.01	1.13	0.51	0.53	0.85
Dy	9.90	10.28	8.31	5.70	6.27	5.96	6.06	7.08	2.86	3.01	5.26
Ho	2.04	2.08	1.67	1.15	1.22	1.17	1.19	1.40	0.55	0.59	1.07
Er	5.79	6.18	4.94	3.13	3.36	3.21	3.33	3.84	1.55	1.63	3.04
Tm	1.02	1.14	0.91	0.53	0.59	0.54	0.58	0.68	nd	nd	nd
Yb	7.04	7.48	6.03	3.43	3.89	3.66	3.69	4.41	1.62	1.80	3.23

Table 1 continued

Samples	WW'1	WW'2	WW'3	WW'4	WW'5	WW'6	WW'7	WW'8	Y2-1	Y2-2	Y1-3
Lu	1.27	1.29	1.04	0.67	0.67	0.63	0.71	0.87	0.41	0.46	0.70
ΣREE	214.38	244.28	216.96	166.11	165.94	141.82	165.38	201.68	102.40	110.80	151.24
LREE/HREE	1.71	1.95	2.23	2.60	2.56	2.18	2.61	2.67	3.74	3.80	3.28
(La/Yb) _N	2.45	2.73	3.71	4.64	4.24	3.10	4.26	4.63	7.29	7.16	5.07
(Gd/Yb) _N	0.85	0.86	0.86	1.26	1.21	1.17	1.25	1.22	1.67	1.56	1.25
δEu	0.78	0.85	0.28	0.79	0.95	1.07	0.96	0.90	0.87	0.86	0.79
δCe	0.97	1.08	0.95	1.01	0.87	0.99	0.98	0.97	0.96	0.96	1.01
Samples	Y1-4	Y1-5	Y1-6	Y1-10	Y1-11	Y1-12	Y1-13	Y1-15	Y1-16	Y1-17	Y1-18
Depth/m	2641	2651	2663	2704	2712	2731	2740	2760	2770	2789	2800
Lithology	Dacite	Andesite	Andesite	Andesite	Andesite	Andesite	Dacite	Rhyolite	Andesite	Andesite	Andesite
SiO ₂	62.23	59.83	60.78	61.33	59.66	61.71	67.43	71.37	61.22	61.97	62.18
Na ₂ O	4.01	3.17	4.60	4.56	4.48	4.15	4.57	4.35	4.54	4.54	4.67
K ₂ O	1.59	1.57	1.1	1.58	1.28	1.33	1.07	1.84	1.6	1.64	1.65
Al ₂ O ₃	16.76	18.82	14.19	14.54	14.83	14.39	13.12	12.43	14.77	14.45	14.9
TFe ₂ O ₃	6.22	7.02	7.47	5.7	6.72	6.56	4.51	3.47	5.74	5.88	5.39
CaO	3.62	3.19	4.85	4.51	5.52	4.66	3.36	1.8	4.54	4.17	4.19
MgO	1.64	1.83	3.12	2.42	2.46	2.59	1.35	1.39	2.55	2.46	2.31
TiO ₂	0.80	1.03	0.82	0.71	0.68	0.68	0.43	0.39	0.72	0.71	0.69
P ₂ O ₅	0.16	0.14	0.13	0.17	0.12	0.14	0.09	0.10	0.17	0.16	0.17
MnO	0.09	0.10	0.13	0.10	0.12	0.12	0.08	0.08	0.11	0.11	0.10
LOI	2.96	3.53	3.03	4.58	4.07	3.8	3.97	2.89	4.26	4.11	3.96
Total	100.08	100.24	100.22	100.21	99.94	100.14	99.99	100.11	100.22	100.20	100.21
Sc	20.3	22.5	21.9	17.1	21	20.2	15.1	13.8	16.7	14	18.4
V	121	148.7	168.7	124.2	133.8	128.2	66.5	42.1	128.3	121.3	119.6
Cr	210.4	174.7	2183	159.8	232.1	225.2	152.2	185.5	110	156.8	151.8
Co	13.6	19	16.6	13.6	18	15.3	8.7	7.8	14.9	13.5	12.2
Ni	34.1	47.3	39.2	66.7	35.4	31.3	20.7	12.4	23.9	63.1	21.4
Cu	53.7	70	57.3	79.1	57.7	48.2	54.1	19	35.3	59	40.6
Zn	140	123.9	79.2	73.8	76.9	72.1	92.4	53.1	66.9	72.7	64.3
Ga	19.1	22.7	16.4	17.5	16.6	16.5	14.8	12.5	17.1	16.8	17.8
Rb	42.6	45.6	23	37.7	26.6	28.3	20.7	17.4	38.9	39.4	39.3
Sr	199.8	170.1	184	266.8	234.6	613.1	189.8	133.9	272.2	265.4	301.5
Zr	178.4	197.3	76.6	114.4	105.1	85.3	126.3	93.2	117.8	128.9	112.6
Nb	9.9	11.6	10.1	7.7	nd	8.4	9	10.1	7.2	6.6	7.9
Ba	354.4	365.8	198.5	325.9	259.6	288.4	186.5	209.5	331.2	341.8	366.4
Hf	5.3	6.1	2.8	3.7	2.8	3	4.5	3.7	3.6	3.8	3.8
Pb	ab	ab	26.1	13.6	ab	ab	ab	25.3	21.5	ab	8.9
Th	6.3	9	nd	5.4	6.4	nd	nd	nd	nd	nd	nd
Sn	74.3	33.13	4.6	6.12	73.39	11.92	54.95	2.77	2.58	11.61	4.45
Cs	1.83	2.51	0.51	1.03	0.86	1.38	0.61	0.38	1.01	1.04	1.15
Ta	0.49	0.54	0.16	0.28	0.22	0.20	0.21	0.12	0.27	0.32	0.26
U	1.49	2.06	0.55	0.96	0.72	0.69	0.69	0.27	0.89	1.09	0.98
Y	24.49	24.20	22.23	20.82	19.25	23.18	34.61	34.96	22.44	21.67	21.56
La	18.48	19.13	8.08	12.40	8.23	9.05	9.32	4.61	11.68	12.72	13.93
Ce	35.89	35.83	17.07	25.65	16.59	19.26	21.93	11.82	24.65	26.44	28.47
Pr	4.78	4.81	2.57	3.62	2.42	2.87	3.38	2.07	3.59	3.68	3.94
Nd	19.75	20.18	12.18	16.06	10.98	13.36	16.17	10.97	16.06	16.21	17.09
Sm	4.26	4.56	3.25	3.78	2.82	3.46	4.51	3.61	3.78	3.81	3.98

Table 1 continued

Samples	Y1-4	Y1-5	Y1-6	Y1-10	Y1-11	Y1-12	Y1-13	Y1-15	Y1-16	Y1-17	Y1-18
Eu	1.11	1.16	1.04	1.04	0.87	1.03	1.17	1.04	1.08	1.02	1.15
Gd	4.20	4.39	3.46	3.65	3.01	3.60	4.79	4.12	3.79	3.73	3.84
Tb	0.75	0.76	0.67	0.66	0.56	0.67	0.96	0.90	0.69	0.68	0.68
Dy	4.66	4.76	4.33	4.12	3.56	4.33	6.37	6.20	4.33	4.19	4.19
Ho	0.95	0.96	0.90	0.83	0.74	0.91	1.35	1.34	0.87	0.85	0.85
Er	2.73	2.70	2.52	2.35	2.11	2.59	3.92	3.95	2.48	2.43	2.39
Tm	nd	nd	nd	nd	nd	nd	nd	nd	nd	nd	nd
Yb	2.99	2.97	2.70	2.46	2.25	2.86	4.45	4.63	2.67	2.67	2.54
Lu	0.59	0.63	0.48	0.48	0.43	0.53	0.85	0.80	0.52	0.52	0.51
ΣREE	125.63	127.03	81.47	97.93	73.82	87.70	113.79	91.03	98.64	100.62	105.13
LREE/HREE	3.04	3.07	2.19	2.77	2.31	2.27	1.99	1.60	2.61	2.74	2.88
(La/Yb) _N	4.43	4.63	2.14	3.62	2.63	2.27	1.50	0.71	3.14	3.41	3.93
(Gd/Yb) _N	1.16	1.22	1.06	1.23	1.11	1.04	0.89	0.74	1.17	1.15	1.25
δEu	0.80	0.79	0.95	0.85	0.92	0.89	0.77	0.83	0.87	0.83	0.90
δCe	0.95	0.93	0.94	0.97	0.95	0.96	1.00	0.99	0.99	1.01	1.01

‘nd’ = no data; ‘ab’ = abnormal data; TFe₂O₃ as total iron, LOI = Loss on ignition, N = chondrite-normalized data, δEu = Eu_N/(Sm_N × Gd_N)^{1/2}, δCe = Ce_N/(La_N × Pr_N)^{1/2}

crystal pyroclasts therein and have sizes of 0.5–1 mm. Most of the tuffs are cemented with volcanic ash and dust.

The secondary alteration, including sericitization of plagioclase and chloritization of hornblende, are commonly observed (Fig. 2h). More importantly, deep diorite and minor granitic xenoliths, comprising mainly of plagioclase, quartz, metamorphic rock debris, and minor hornblende glomerocrysts, are seen throughout the Carboniferous volcanic sequence of well Y-1 (Fig. 2i) but are rare in well Y-2 and outcrop WW’.

5 Geochemistry

5.1 Major elements

The collected samples showed a medium to high LOI (0.42%–6.73%), and all the major oxides were LOI-free normalized before petrogenetic interpretation. In general, high-field-strength elements (HFSEs; e.g., Ti, Ta, Zr, and heavy REEs (HREEs)) exhibit low mobility. This makes them useful for petrographic classification and petrogenesis (Pearce and Cann 1973; Pearce and Norry 1979). The Carboniferous volcanic rocks in the northern Luliang Uplift considered herein consist of varying contents of SiO₂ (50.24 wt.%–75.52 wt.%), total alkali (Na₂O + K₂O = 4.22 wt.%–8.27 wt.%), Al₂O₃ (12.03 wt.%–18.82 wt.%), MgO (0.3 wt.%–4.19 wt.%), CaO (0.36 wt.%–8.36

wt.%), TFe₂O₃ (1.67 wt.%–11.21 wt.%), TiO₂ (0.12 wt.%–2.63 wt.%), and P₂O₅ (0.03 wt.%–0.83 wt.%). They are plotted in the SiO₂–Na₂O + K₂O diagram, and fall in the basalt, andesite, dacite, and rhyolite fields, and outcrop WW’ lacks intermediate volcanic rocks (Fig. 3a). Furthermore, in the Nb/Y–Zr/TiO₂ diagram (Fig. 3b), the major rocks in well Y-1 fall in the andesite field, and rocks from outcrop WW’ fall in the rhyolite, trachyandesite, basalt, and alkali-basalt fields. Importantly, the volcanic rocks from outcrop WW’ indicate an obvious bimodal nature. Moreover, the SiO₂–K₂O diagram shows that the rocks in well Y-1 plot mainly as calc-alkaline assemblages, but those in well Y-2 correspond to high-K assemblages (Fig. 4a). The basaltic volcanic rocks from outcrop WW’ are low–high-K assemblages; however, the acid rocks plot in a high-K field. The Ta/Yb–Th/Yb diagram confirms that these rocks originated from calc-alkaline assemblages, excluding one rock in well Y-1 (Fig. 4b). In the Harker diagrams, MgO, Al₂O₃, CaO, TFe₂O₃, TiO₂, and P₂O₅ show negative relationships with SiO₂; however, K₂O shows a slight positive relationship with SiO₂, and there is no significant relationship between Na₂O and SiO₂ (Fig. 5). Interestingly, the samples in well Y-1 form a different branch to the main tendency in five diagrams, but they exhibit a high consistency with other samples in TiO₂, TFe₂O₃, and MgO diagrams. Although some branches exist, most samples in well Y-1 fall in the main tendency composed of the samples from well Y-2 and outcrop WW’.

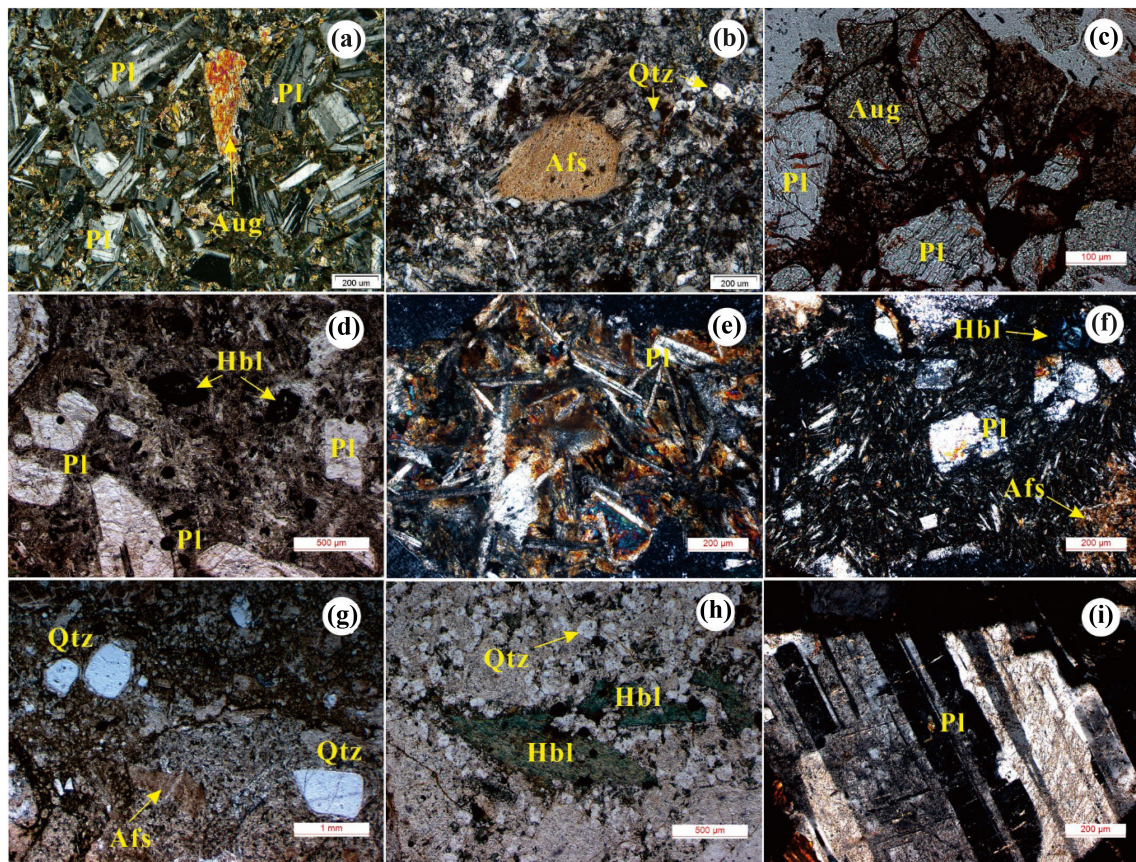


Fig. 2 Representative microphotographs of the Carboniferous volcanic rocks from well Y-1, Y-2, and outcrop WW' from the northern Luliang Uplift. **a** basalt, 1950 m in the outcrop WW'; **b** rhyolite, 670 m in the outcrop WW'; **c** pyroxene andesite, 3876 m in well Y-2; **d** hornblende andesite, 3480 m in well Y-2; **e** basaltic andesite, 2611 m in well Y-1; **f** dacite, 2731 m in well Y-1; **g** dacite tuff, 2740 m in well Y-1; **h** crystal tuff with chloritization of hornblende, 2679 m in well Y-1; **i** Carlsbad bicrystals of plagioclase, 2800 m in well Y-1. Pl-plagioclase; Aug-augite; Qtz-quartz; Afs-alkali-feldspar; Hbl- hornblende

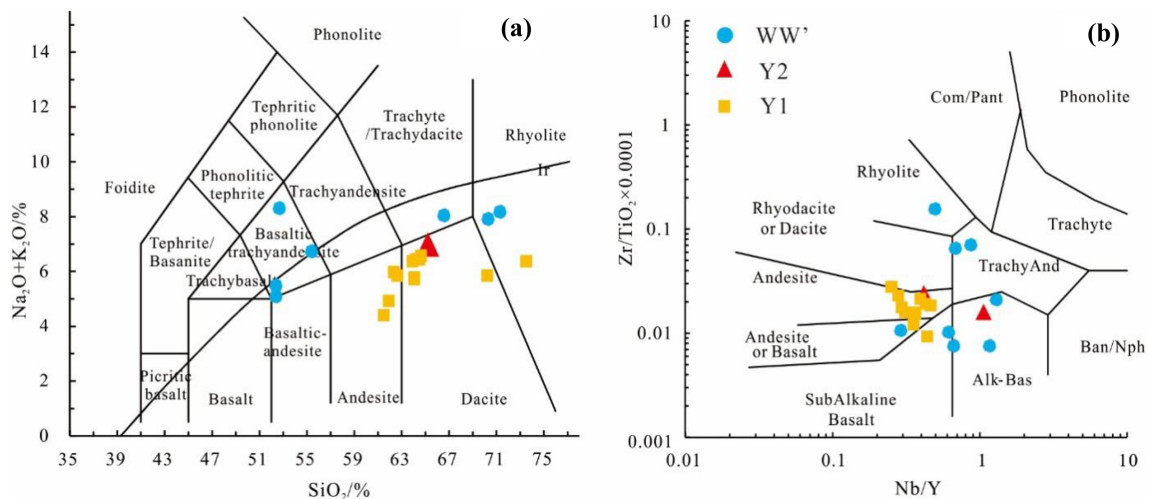


Fig. 3 Geochemical classification of the Carboniferous volcanic rocks from the northern Luliang Uplift. **a** $\text{SiO}_2\text{-Na}_2\text{O} + \text{K}_2\text{O}$ diagram (Le Maitre et al. 1989); **b** Nb/Y-Zr/TiO_2 diagram (Winchester and Floyd 1977)

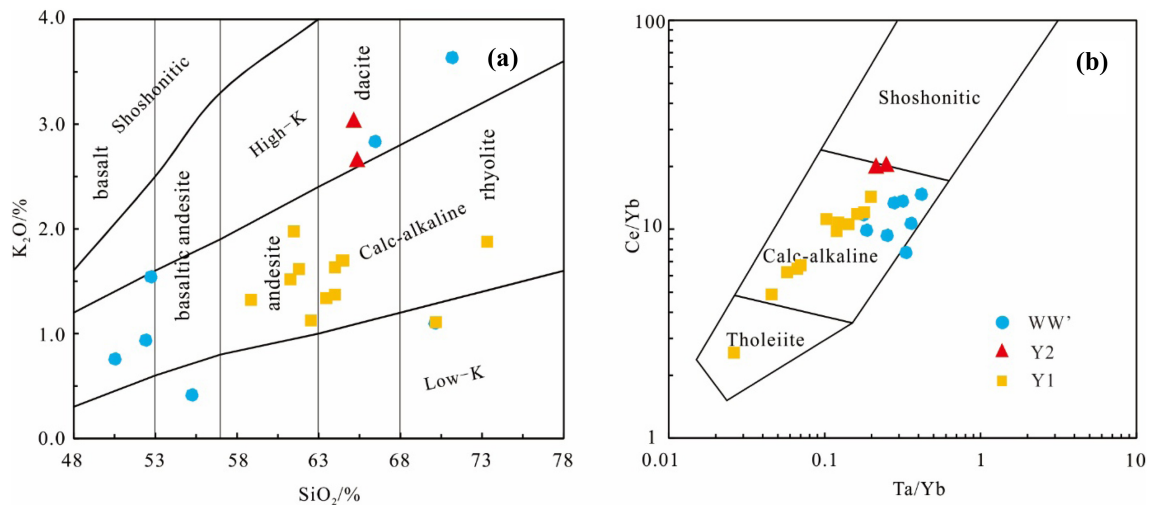


Fig. 4 Discrimination diagrams of volcanic magma series of the Carboniferous volcanic rocks from the northern Luliang Uplift. **a** SiO_2 - K_2O diagram (Ewart 1982); **b** Ta/Yb - Ce/Yb diagram (Pearce 1982)

5.2 Trace elements

The total REE concentrations of the 22 volcanic rock samples vary widely from 73.82 to 244.28 ppm. Samples in outcrop WW' show higher REE concentrations (141.82–244.28 ppm); nonetheless, samples in wells Y-1 and Y-2 show lower REE concentrations (73.82–151.24 ppm). All these rocks exhibit various chondrite-normalized REE patterns that are characterized by slightly right-skewed trends (Fig. 6a), namely relative enrichment of LREE ($\text{La}_\text{N}/\text{Sm}_\text{N} = 0.83$ –3.40; $\text{La}_\text{N}/\text{Yb}_\text{N} = 0.71$ –7.29), slight negative or no Eu anomalies ($\delta\text{Eu} = 0.77$ –1.07, except for WW'-3 which has a particularly low value of 0.28), and slightly negative or no Ce anomalies ($\delta\text{Ce} = 0.87$ –1.08). The REE patterns of the rocks in well Y-2 are similar to those in well Y-1, but differ from those in outcrop WW'. The REE patterns of rocks from outcrop WW' present lower LREE/HREE ratios, and the basalts show no significant variation in Eu anomaly. The negative Eu anomalies in some intermediate volcanic rocks of wells Y-1 and Y-2 indicate that plagioclase fractionation played an important role in their evolution. Moreover, all these samples exhibit $\text{La}_\text{N}/\text{Yb}_\text{N}$ ratios ranging from 0.71 to 7.29, lower than that of OIB (12.29) and higher than that of normal mid-ocean ridge basalt (N-MORB) (1.0) (Sun and McDonough 1989). Spider diagrams of samples from outcrop WW' show a chaotic distribution, but they can still be divided into two groups according to the depletion in some HFSEs (Nb, P, and Ti). The spider diagrams for samples from wells Y-1 and Y-2 are similar to each other and indicate enrichment in large ion lithophile elements (LILEs, e.g., Rb, Ba, and K) and depletion in HFSEs (U, Nb, Ta, P, and Ti) (Fig. 6b). These features are distinct from those of N-MORB and OIB. However, some Th and Sr anomalies can be observed in the samples from well Y-1. Furthermore, most basalts from outcrop WW' show the presence of Nb element ($\text{Nb} =$

8.9–19.6 ppm) consistent with Nb-enriched basalts ($7 \text{ ppm} < \text{Nb} < 20 \text{ ppm}$) affected by melting of the metasomatized mantle (Defant 1992; Martin et al. 2005).

6 Discussion

6.1 Spatial and temporal distribution of the Carboniferous volcanic rocks in the northern Luliang uplift

The distribution of the Carboniferous volcanic rocks across the western Luliang Uplift is complex (Zhang et al. 2008a). Basic–ultrabasic volcanic rocks occur in the Madong area (Li et al. 2015b), granitoid plutonites and bimodal volcanic rocks occur in the Shixi area (Wang et al. 2002; Chen et al. 2010), and andesite–dacite associations are found in the Shiyintan area (Zhang et al. 2018). The gravity and magnetic anomalies detected in the Shiyintan High are stronger than those in its northern and southern sides, implying possible arc-like andesite–dacite zone (Fig. 2, Han et al. 2019b). The Carboniferous lithology preserved in the eastern Luliang Uplift is comparatively simple and mainly consists of basalt, pyroclastic rock, and minor rhyolite emplaced in a post-collisional extensional setting (Wu et al. 2009; Su et al. 2012). Moreover, the gravity and magnetic anomalies also indicate the possibility of the distribution of the mafic–ultramafic complexes in the eastern Luliang Uplift (Fig. 8, Li et al. 2015a). Discoveries of paleontological fossils (e.g. sporopollen fossil and *Spirifer subgrandis* Rotai) collected from outcrop WW' indicate an Early Carboniferous formation age (cited from unpublished results from the Geological Scientific Research Institute, Shengli Petroleum Administration).

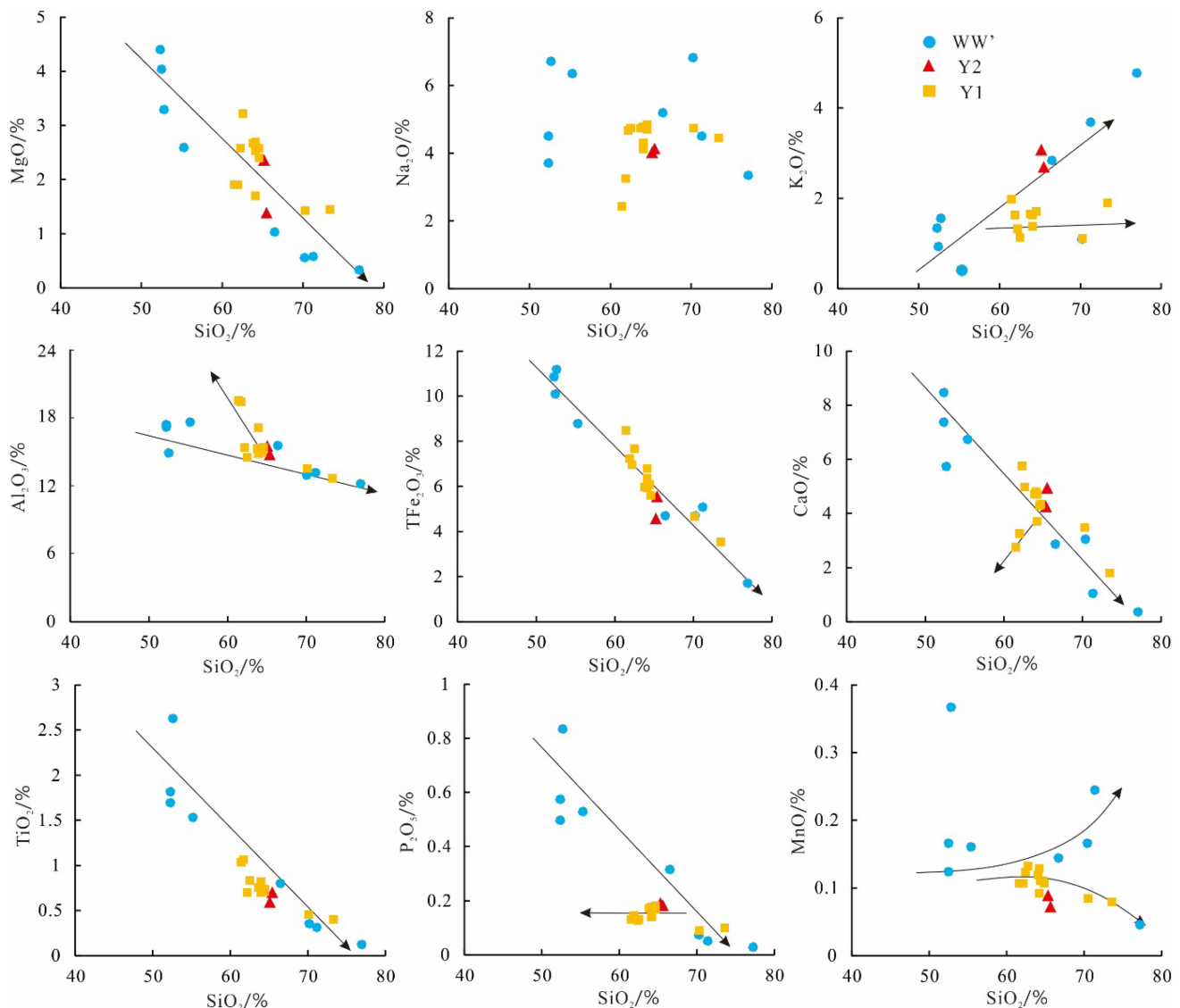


Fig. 5 Major elements Na_2O , K_2O , Al_2O_3 , TFe_2O_3 , CaO , MgO , TiO_2 , P_2O_5 , and MnO versus SiO_2 for the Carboniferous volcanic rocks from the northern Luliang Uplift

Previous studies on outcrop WW' also indicate that its intermediate-acid volcanic rocks formed in the Early Carboniferous (332–336 Ma), and record some island-arc signatures (Xiao et al. 2011). Furthermore, the eastern Luliang arc and East Junggar have been interpreted to have evolved into a post-collisional and then an intraplate extensional setting from the middle of the Early Carboniferous, causing post-collisional volcanic rocks and intraplate volcanic rocks to be emplaced widely (Zhang et al. 2015a, b).

A few wells have been drilled in the Shiyintan area, and only wells Y-1 and Y-2 have been reported. Notably, the volcanic rocks from these two wells show similar petrographic and geochemical characteristics, comprising intermediate-acid basaltic andesite–andesite–dacite assemblages. Interestingly, the rocks in well Y-1 tend to be

low-K calc-alkaline assemblages; however, the rocks in well Y-2 are high-K to shoshonitic assemblages (Han et al. 2019b). New geochronological results indicate that the andesite–dacite associations in well Y-2 erupted during the Late Carboniferous (303 ± 7.7 Ma, Han et al. 2019a; 310.6 ± 6.0 Ma, Han et al. 2019b; 310.8 Ma, Zhang et al. 2018). However, even more investigations suggest that the eruption of the volcanic rocks in well Y-1 occurred during the Early Carboniferous. For example, Mao (2012) reported two eruption ages 353.1 ± 2.7 and 311.7 ± 5.1 Ma, for these volcanic rocks. Noteworthy, a limited number of zircons were analyzed for the Late Carboniferous. Yang and Chen (2016) synthesized the formation ages of Carboniferous volcanic rocks in well Y-1. The results demonstrated the age with the most selective confidence interval in the Early Carboniferous (356 Ma). The

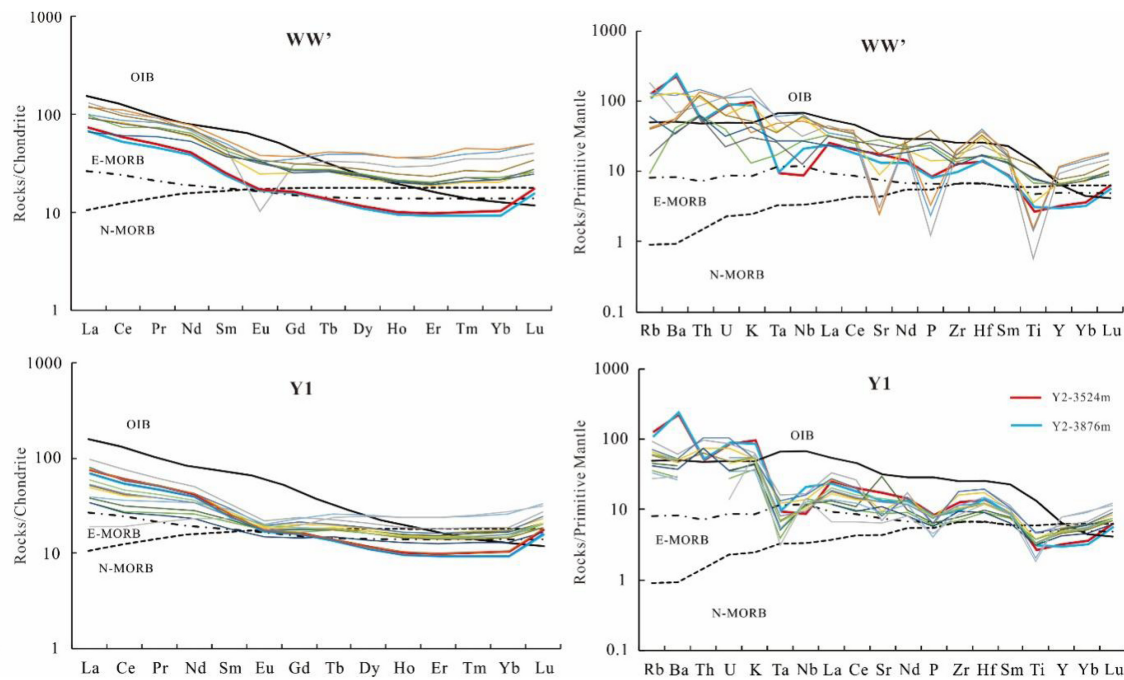


Fig. 6 Chondrite normalized REE patterns **a** and primitive mantle normalized trace element spider diagrams **b** for the Carboniferous volcanic rocks from the northern Luliang Uplift. OIB, N-MORB, E-MORB, chondrite, and primitive mantle normalized values according to Sun and McDonough (1989)

occurrence of minor Devonian zircon is a result of the widespread presence of deep xenoliths (Fig. 2i). Although wells Y-1 and Y-2 are geographically close to each other, the significantly higher K, Rb, and Ba contents in well Y-2 imply that the formation age of the rocks in well Y-1 is earlier than the age of those in well Y-2. This is attributed to the fact that deeper subduction leads to more melting of continental material, which is then introduced into island arc magma (Zhao et al. 2004). Therefore, it is suggested herein that the low-K calc-alkaline volcanic rocks in well Y-1 were emplaced in the Early Carboniferous. Many investigations on Carboniferous volcanic rocks in the eastern Luliang Uplift have been carried out, and they have mainly reported mafic volcanic rocks with within-plate extensional characteristics. The eruption ages of these volcanic rocks range from the late part of the Early Carboniferous to the Late Carboniferous. For example, Li et al. (2015a) reported new high-precision zircon U–Pb ages for basalts of 308.6 ± 4.7 Ma (SIMS) and 337.2 ± 4.1 Ma (SHRIMP) in the eastern Luliang Uplift.

6.2 Geochemical differences among volcanic rocks in well Y-1

Although Han et al. (2019b) suggested the occurrence of a geochemical transition between 2700 and 2750 m in well Y-1, it is significant to note that new results show little or no variation in the lower volcanic rocks (> 2660 m)

(Fig. 7). This observation can be supported based on the mineral contents: the upper volcanic rocks have more pyroxene without quartz, and the lower volcanic rocks have more quartz and orthoclase. The first observation of quartz and orthoclase was made at a depth of 2651 m. Geochemical indicators can also assist in observing the transition. For example, normal arc intermediate-acid volcanic rocks present low, but coherent TiO_2 (0.5%–0.83%) and Zr (< 130 ppm) concentrations (Xia 2014; Pearce 1982). These critical values are in accordance with the lower volcanic rocks in well Y-1 ($0.39\% < \text{TiO}_2 < 0.82\%$; $76.6 \text{ ppm} < \text{Zr} < 128.9 \text{ ppm}$). The geochemical stratigraphy allows the rocks to be divided into two parts according to the tendency from being upright to inclined as shown in Fig. 7. The transition depth of 2660 m can be discerned in this geochemical stratigraphy, which is consistent with the mineral observations. The transition suggested by Han et al. (2019b) cannot be always discerned in the profiles. However, a significant change has occurred by the time the upper volcanic rocks were emplaced: these rocks are similar to basaltic andesite. The higher HFSEs (Ti, Ta, and Zr) and HREEs (LREE/HREE and $(\text{La}/\text{Yb})_N$) in the upper volcanic rocks compared to those in the lower volcanic rocks in well Y-1 may suggest melting of the mantle wedge. Moreover, the upper volcanic rocks in well Y-1 show higher La/Sm and Zr/Y ratios (Fig. 7), which indicates a higher degree of continental crust involvement (Pearce and Mei 1990; Shellnutt et al. 2012). Smaller

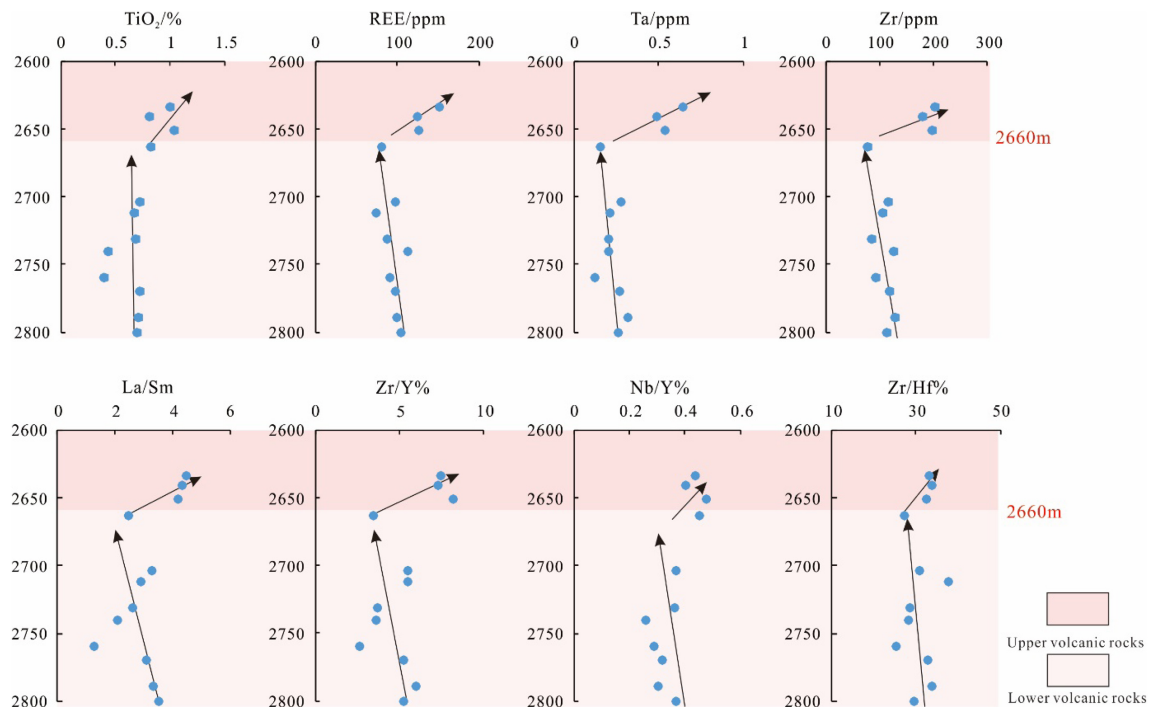


Fig. 7 Selected geochemical data in the Lower Carboniferous volcanic rocks from well Y-1 showing a geochemical transition

differences could be observed between the upper and lower volcanic rocks in the profile including Nb/Y and Zr/Hf ratios. However, a decrease of these ratios in the lower volcanic rocks suggests they were more likely derived from the magmatic source with a stronger melting of oceanic crust (Bolge et al. 2006; Luo et al. 2016).

During subduction, the overlying mantle wedge was commonly modified by the addition of materials from the subducting slab, including fluids and slab melts. Spider diagrams of volcanic rocks in well Y-1 show a binary distribution. The upper volcanic rocks show some depletion or no change in HFSEs, and the lower volcanic rocks show depletion of Ta, Nb, and Ti but the enrichment of Th, Zr, and Hf. These findings indicate that subducted sediments played a significant role in the formation of these island arc volcanic rocks. Figure 8a demonstrates fluid enrichment of both the upper and lower Y-1 andesites and dacites, and this indicator is more significant for the lower volcanic rocks. However, higher differentiation between LREEs and HREEs in the upper volcanic rocks (based on LREE/HREE and La_N/Yb_N values) and the similarity of their REE content to OIB indicate more input of fluid and/or melt components from the oceanic crust into the magmatic source. This is also supported by the Nb/Y vs. Rb/Y diagram (Fig. 8b), which suggests the involvement of both fluid and melt. The finding that the upper rocks in well Y-1 have higher La/Yb ratios (6.18–7.06) than the lower rocks (1.00–5.48), though not as extreme as many so-called adakites, might be interpreted as reflecting the involvement

of slab melts (Walowski et al. 2015). The higher Nb/Y values of the upper Y-1 rocks are also indicative of the addition of slab melts, playing an increasingly important role in these arc-type calc-alkaline magmas. Furthermore, their geochemical ratios (La/Yb and Nb/Y) are similar to those of Y-2 volcanic rocks, which have been shown to have been significantly affected by the melting of the subducted slab (Han et al. 2019a). Therefore, it was proposed herein that the volcanic rocks in well Y-1 may share the arc-related magmatic signal but that slab melts played a larger role in the upper volcanic rocks.

6.3 Petrogenesis

6.3.1 Post-magmatic alteration

These volcanic rocks have relatively variable LOI values (0.42%–4.97%), suggesting that the samples might have suffered varying degrees of low-temperature alteration. The volcanic rocks in wells Y-1 and Y-2 and at outcrop WW' show low to moderate values of LOI (0.42%–4.97%). Petrographic observations also revealed some alteration of volcanic rocks in well Y-1. To detect whether elements were mobilized at the whole-rock scale, bivariate plots of Zr vs. representative trace elements were applied herein (Fig. 9). For well Y-1, selected HSFEs (Hf and Ta), mobile elements (Ba and K), and REEs (La and Y) displayed good correlations with Zr, indicating only slight or no secondary alteration (He et al. 2008; John et al. 1982). Furthermore, Nb also

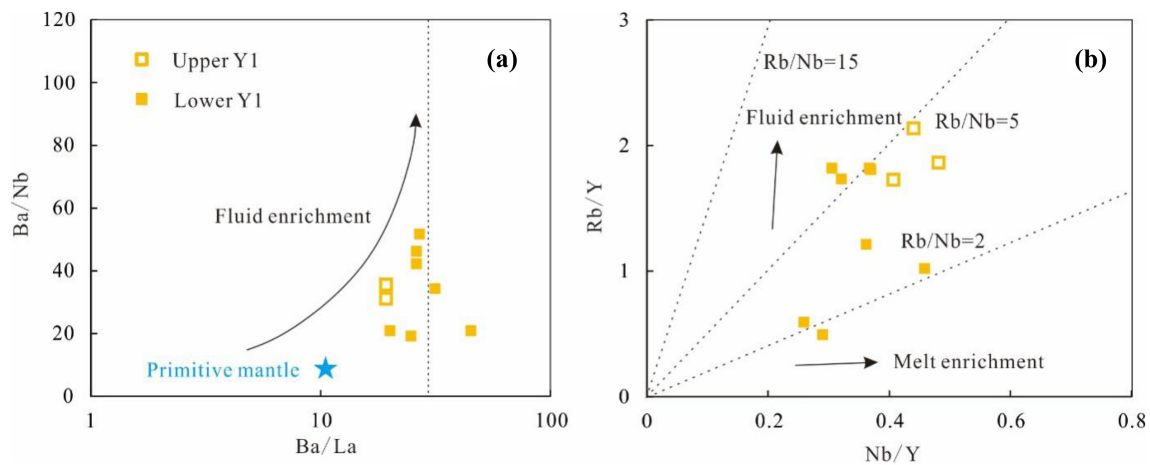


Fig. 8 Diagrams of Ba/La vs. Ba/Nb **a** and Nb/Y vs. Rb/Y **b** indicate fluids and slab melts addition

exhibited a strong correlation with Th, U, Ba, Sr, Ta, and La. However, these elements display chaotic distributions, in particular, the mobile elements from outcrop WW'. Therefore, it is suggested that post-magmatic alteration did not have a significant effect on the composition of the rocks from well Y-1, but some low-temperature alteration occurred in the bimodal volcanic rocks from outcrop WW', which may be associated with chemical weathering.

6.3.2 Magma sources

6.3.2.1 (1) Basalt The basalts from outcrop WW' have a low SiO₂ (50.28%–53.97%) content, a low to moderate Mg# (0.37–0.46) value. Moreover, their Cr (33–135.1 ppm) and Ni (27.1–83.1 ppm) concentrations are lower than those of the primary mantle-derived magmas (Cr = 300–500 ppm, Ni = 300–400 ppm, Frey et al. 1978), indicating that the magma experienced significant crystal fractionation after originating from the mantle. The obvious negative relationships among MgO, CaO, and TFe₂O₃ and SiO₂ are compatible with pyroxene fractionation (Fig. 5). The high Al₂O₃ (15%–17.21%) content, together with the negative Eu and Sr anomalies suggests some fractionation of plagioclase. Moreover, the significant negative correlation between Dy/Yb and SiO₂ indicates amphibole fractionation, as they result from preferential incorporation of Dy over Yb (Garrison and Davidson 2003). The presence of positive P–Hf anomalies, but slightly negative Nb–Ta anomalies within the spider diagrams for the basalts suggests the assimilation of some crustal material in these magmas during ascent. Their high Th/Ce (0.2 and 0.23) and Th/La (0.43 and 0.54) ratios also indicate significant crustal contamination during the generation of the magmas. This is ascribed to the fact that the continental crust has relatively high Th/Ce (< 0.15, Taylor and McLennan 1995) and Th/La (< 0.30, Plank 2005)

ratios, while mantle-derived magmas have low Th/Ce (0.02–0.05) and Th/La (< 0.12) ratios (Sun and McDonough 1989).

These basalts show no significant LILE-enrichment or HFSE-depletion, suggesting their derivation from various mantle sources, which is inconsistent with Late Carboniferous basalts in the same areas (Li et al. 2015a). This is also supported by (Ta/La)_{PM} vs. (Hf/Sm)_{PM} (Fig. 10a) and Zr vs. Nb (Fig. 10b) diagrams. This evidence indicates that the magmatic sources of the basalts were complex, originating from depleted mantle to enriched mantle blended with fluids or melts from a subducted slab. Their trace elements are inconsistently distributed, and opposing LILE and HFSE anomalies can be discerned in the multi-element diagrams (Fig. 6), which also indicates the existence of various mantle sources. Asthenosphere-derived mafic rocks commonly show low La/Nb (< 1.5) and La/Ta (< 22) ratios, whereas those of rocks derived from the lithosphere are higher (Fitton et al. 1988). The basalts from outcrop WW' show various La/Nb (0.66–2.46) and La/Ta (14.61–32.96) ratios, also indicating an important role for lithospheric materials in their magmatic source. Their flat chondrite-normalized HREE patterns and relatively low HREE and Y content might reflect the influence of residual garnet during partial melting in the lower crust (Genç and Tüysüz 2010). The basalt samples exhibit low Sm/Yb and La/Yb ratios, which is consistent with a spinel–garnet-bearing mantle source that has undergone 10% partial melting to generate a primary basaltic magma (Fig. 10c).

6.3.2.2 (2) Intermediate-acid volcanic rocks The rhyolites and dacites from outcrop WW' are all characterized by high SiO₂ and Na₂O + K₂O contents, low TFe₂O₃ and MgO contents, strong or slightly negative Eu anomalies (0.28–0.87), and relatively high Ga/Al ratios (1.0–2.0) and Zr (164.9–227.2 ppm), Nb (22.3–46.1 ppm), Ce

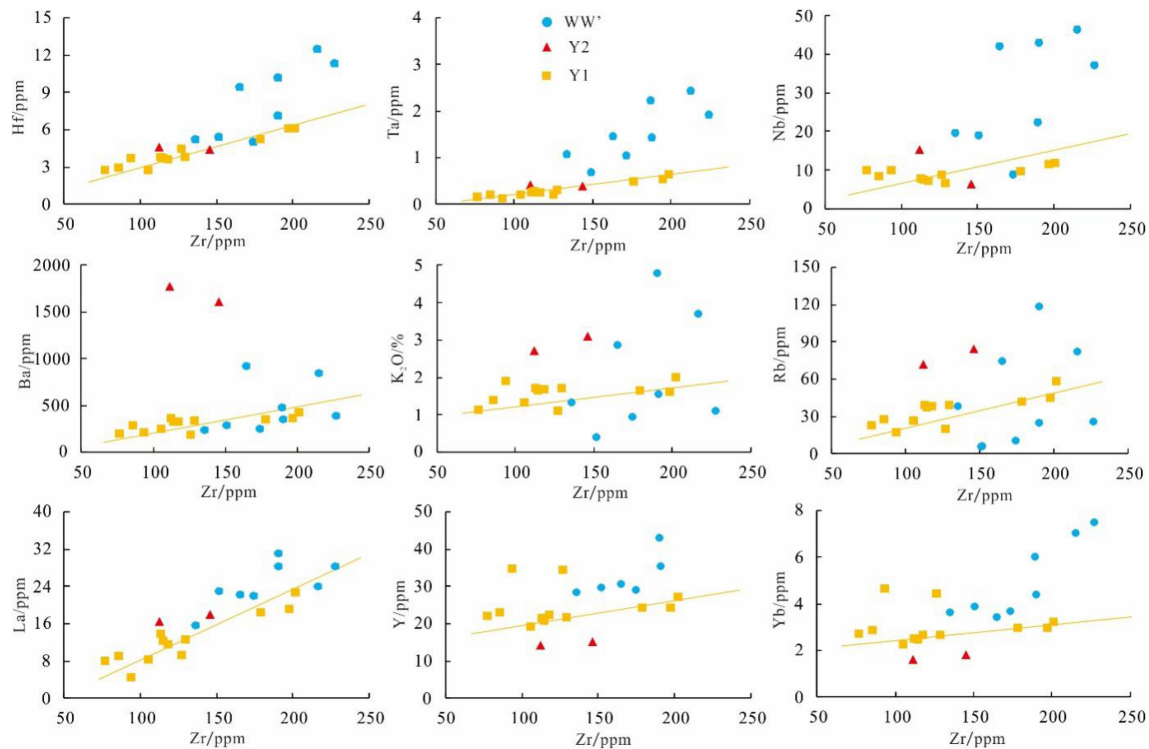


Fig. 9 Bivariate plots of Zr vs. representative HFSE (Hf, Ta, and Nb), LILE (Ba, K, and Rb), and REE (La, Y, and Yb) for volcanic rocks in the northern Luliang Uplift

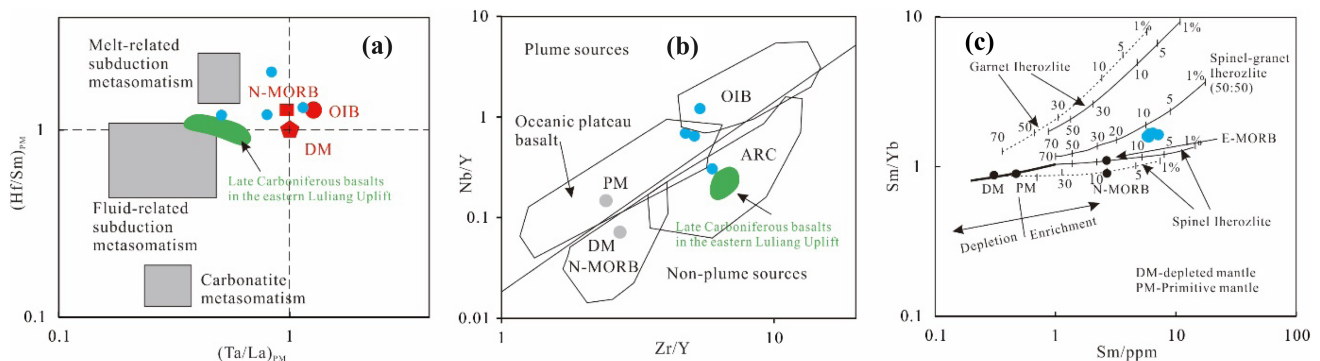


Fig. 10 Diagrams of **a** $(\text{La}/\text{Sm})_{\text{PM}} - (\text{Hf}/\text{Sm})_{\text{PM}}$ (La Flèche et al. 1998), **b** $\text{Zr}/\text{Y} - \text{Nb}/\text{Y}$ (Condie 2005) and **c** $\text{Sm}/\text{Yb} - \text{Sm}$ (Aldanmaz et al. 2000) indicate the magma source of basalts in the outcrop WW'. The Late Carboniferous basalts in the eastern Luliang Uplift are derived from Li et al. (2015a)

(50.67–69.24 ppm), and Y (30.63–52.67 ppm) concentrations compared to those in wells Y-1 and Y-2. These characteristics indicate that the samples in outcrop WW' share affinities with A-type granites (Whalen et al. 1987). Furthermore, major element Harker variation diagrams and trace element distribution patterns show significant differences between the intermediate-acid volcanic rocks from outcrop WW' and from wells Y-1 and Y-2. This is probably attributed to the difference in their magma sources. For felsic rocks in bimodal volcanic rock assemblages, the generation of silicic magmas can be attributed to the following two mechanisms: (1) fractionation of coeval

basaltic magma and (e.g., Tian et al. 2010) and (2) melting of the felsic crust (e.g., Brewer et al. 2004). The different distributions of trace elements between mafic and felsic rocks in the bimodal volcanic rocks and no existence of intermediate volcanic rocks argue against the differentiation of coeval basalt parent magmas.

The samples in outcrop WW' and well Y-1 consist of low Sr (51–382 ppm, average: 222.36 ppm) and Na_2O ($\text{K}_2\text{O}/\text{Na}_2\text{O} = 0.19\text{--}1.42$, average: 0.5) concentrations and Sr/Y (0.97–25.38, average: 10.19) and $(\text{La}/\text{Yb})_{\text{N}}$ (2.45–7.29, average: 3.64) ratios and high Y (14.11–52.67 ppm, average: 27.93 ppm) and Yb (1.62–7.48 ppm, average: 3.55 ppm)

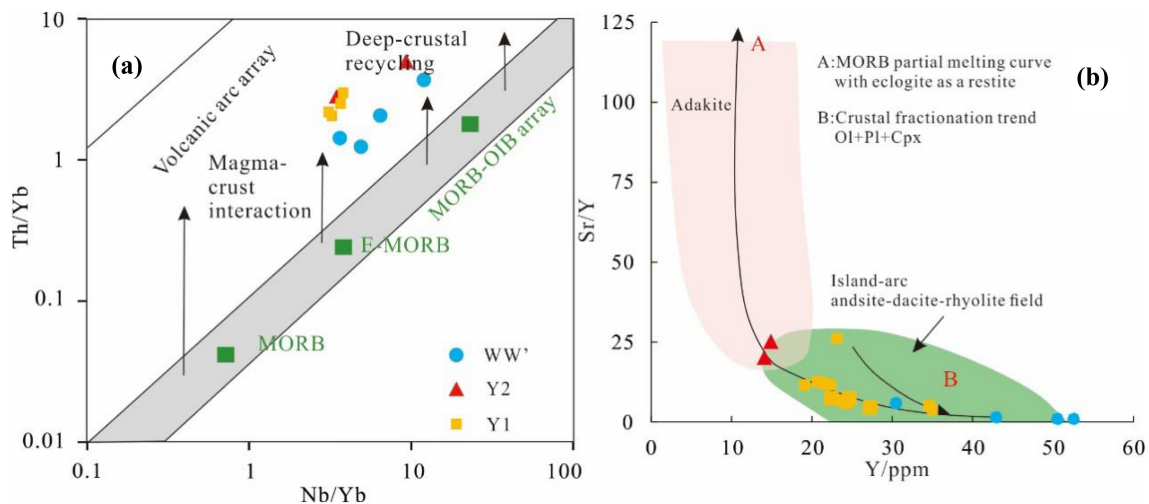


Fig. 11 Diagrams of **a** Nb/Yb–Th/Yb (Pearce 2008); **b** Y–Sr/Yb (Defant and Drummond 1990) indicate the magma source of intermediate-acid volcanic rocks in the northern Luliang Uplift

concentrations, similar to normal calc-alkaline granitoids derived from pre-existing juvenile crustal materials (Yang et al. 2016). Furthermore, the Nb/Yb–Th/Yb diagram also indicates that these intermediate-acid volcanic rocks originated from a subduction-related crustal anatexis and share some arc signatures (Fig. 11a). The samples obtained from wells Y-2 and Y-1 share increasingly significant affinities with arc-type calc-alkali volcanic rocks, reflected by their LILE-enrichment and HFSE-depletion. This is also supported by the Y–Sr/Y diagram, in which they show significant similarity to island arc-type volcanic rocks derived from crustal fractionation (Fig. 11b). The higher Nb/Yb (3.56–12.19) and lower Yb/Ta (2.37–4.62) ratios of the felsic rocks exhibit similarities to crust that plots between OIB and IAB, whereas those in wells Y-1 (Nb/Yb: 2.02–3.91; Yb/Ta: 5.05–38.58) show stronger associations with arc-type volcanic rocks (Eby 1992; Pearce 2008). Therefore, the Carboniferous intermediate-acid volcanic rocks in the northern Luliang Uplift showed a strong association with arc-type calc-alkali basaltic magma and were probably generated by the partial melting of the juvenile basaltic lower crust, associated with mantle-derived melts. However, these volcanic rocks in outcrop WW' have a low Mg# value (0.17–0.3), suggesting weak involvement of mantle materials.

6.4 Implications for the Carboniferous tectono-magmatic evolution of the northern Luliang Uplift

6.4.1 East–west differences in the tectonic environment of the northern Luliang Uplift during the Carboniferous

The different petrographies of volcanic rocks across the northern Luliang Uplift indicate the possibility of their

formation in different tectonic settings. The typical bimodal volcanism in the eastern part of the northern Luliang Uplift suggests a continental extensional setting; in contrast, the arc-type volcanic rocks in the Shiyintan area in the west imply ongoing subduction. The geochemical character of the latter Carboniferous high-K calc-alkali volcanic rocks is also consistent with that of the arc volcanic rocks, as they show LILE-enrichment and depletion in Nb, Ta, P, and Ti, which is indicative of the formation of subduction-related rocks in an island arc environment (Grove et al. 2003). Tectonic setting discrimination diagrams were used for basaltic rocks and acid rocks, respectively, to further interpret their tectonic environments.

On an Nb × 2–Zr/4–Y diagram, three samples fall in the field of within-plate basalt, and one sample falls in a possible volcanic arc basalt field (Fig. 12a). However, the association of the one samples in the C field with the Late Carboniferous basaltic rocks investigated by Li et al. (2015a) indicates that they were the products of extensional geodynamics. This is also supported by the Zr–TiO₂ diagram (Fig. 12b). Moreover, these basalts have low Al₂O₃ concentrations (15.00%–17.21%) and low Ba/La (11.47–12.74) ratios and high TiO₂ (1.50%–2.63%) concentrations and Ta/Hf (0.13–0.20) and Ti/V (44–86) ratios, similar to those of within-plate basalts rather than typical arc basalts (Pearce 1982; Condie 1989; Ajaji et al. 1998; Xia 2014). On the Zr/Y versus Zr diagram, the basaltic rocks plot in the within-plate basalt field (Fig. 12c), indicating that they share a geochemical association with within-plate basalts and were likely formed in an extensional setting.

The intermediate-acid volcanic rocks exhibit significant differences in their specific tectonic setting discrimination diagrams, related to their binary nature. This difference is

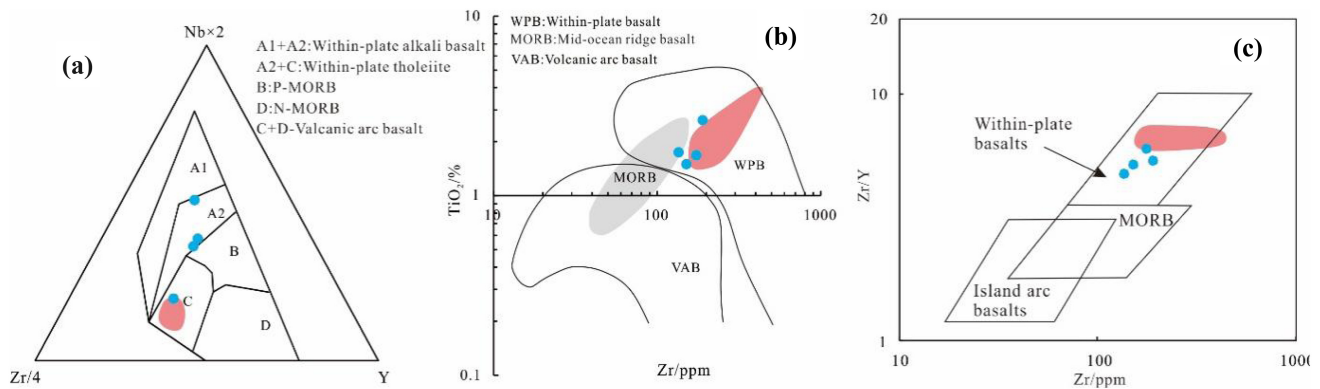


Fig. 12 Tectonic setting discrimination diagram for the basalt. **a** $Nb \times 3-Zr/4-Y$ diagram (Meschede 1986); **b** $Zr-TiO_2$ diagram (Pearce and Cann 1973); **c** $Zr-Zr/Y$ diagram (Pearce and Norry 1979). The Late Carboniferous basalts (the red areas) in the eastern Luliang Uplift are derived from Li et al. (2015a)

associated with the geographical location and eruption age, as they indicate contrary dynamics. The most acidic volcanic rocks from outcrop WW' fall in the within-plate basalt field, consistent with the conclusions regarding basalts (Figs. 12a, b) and suggesting that they erupted in an extensional setting. One dacite shares some association with arc volcanic rock, probably resulting from the inheritance of arc volcanic rocks before the collision (Mao et al. 2010; Wu et al. 2009). However, the intermediate volcanic rocks in the Shiyintan area (wells Y-1 and Y-2) universally plot in the volcanic arc granite field (Figs. 13a, b), suggesting that their tectonic environment was a typical volcanic arc during subduction. Although the lower volcanic rocks in well Y-1 fall in the oceanic arc field (Fig. 13c), their high Nb (9.9–11.9 ppm) concentration, and the Th/Yb (2.11–3.03) and Th/Y (0.26–0.37) ratios, which differ from those of an oceanic arc, indicate that they were formed in a continental arc and that their mantle source was metasomatized by melting of subducted oceanic crust (Pearce 1983). This is also in agreement with the above-mentioned results regarding vertical geochemical changes in well Y-1, which indicates a higher melting of the mantle in the lower volcanic rocks.

6.4.2 Implications for the tectono-magmatic evolution of the northern Luliang Uplift

As discussed above, the volcanic rocks in the eastern and the western parts of the northern Luliang arc exhibit evidence for different magmatic origins in settings with opposing geodynamics. Lower Carboniferous bimodal volcanic rocks in outcrop WW', along with observations of A-type granites (Han et al. 2006), indicate that after the closure of the eastern part of the Keramaili oceanic basin, the eastern part of the Luliang arc became an intra-continental rift setting during the Early Carboniferous (Fig. 14a). Furthermore, crustal extension and thinning resulted in the upwelling of lithospheric mantle metasomatized to different degrees by arc-type magma, causing magma underplating. The upwelling of these hot calc-alkali basaltic magmas further resulted in the partial melting of the lower crust. Consequently, the calc-alkali basalt experienced some crustal contamination, and intermediate-felsic eruptions accompanied the basalts. During the Late Carboniferous, slab rollback of the Junggar Oceanic crust contributed to stronger extension in the Luliang arc, causing higher degrees of partial melting of metasomatized wedge mantle by hydrous fluids and melts from subducted

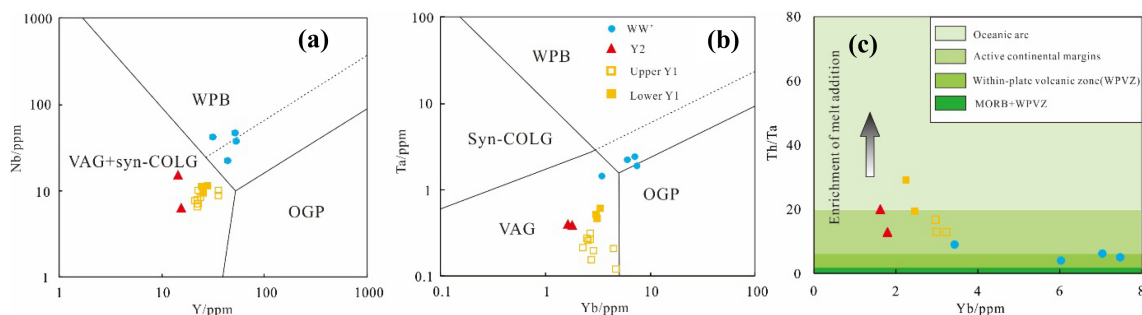


Fig. 13 Tectonic setting discrimination diagram for the intermediate-acid volcanic rocks. **a** $Y-Nb$ diagram (Pearce et al. 1984); **b** $Yb-Ta$ diagram (Pearce et al. 1984); **c** $Yb-Th/Ta$ diagram (Gorton and Schandl 2000)

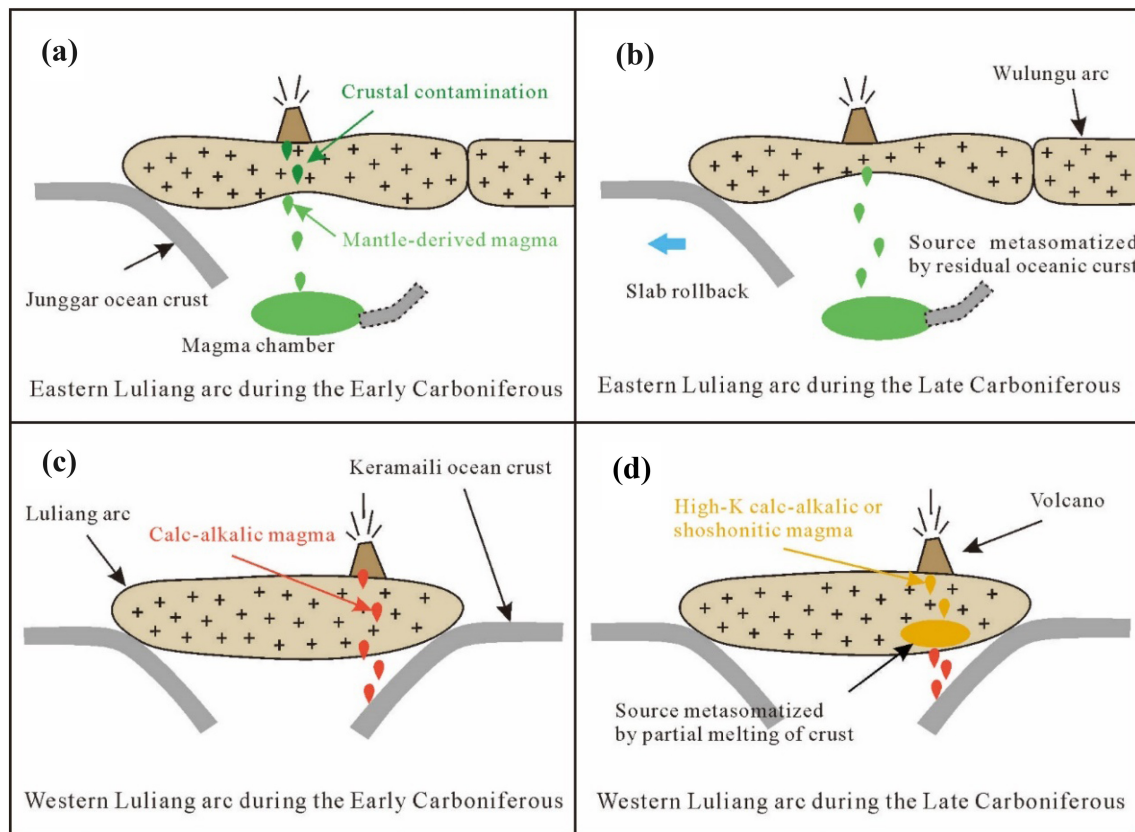


Fig. 14 The different tectonic settings and magmatic geodynamics between eastern and western parts of the Luliang arc during the Carboniferous

sediments (Fig. 14b, Li et al. 2015a). The Carboniferous low-K to high-K volcanic rocks preserved in the Shiyintan area indicate subduction and a continental arc environment in the western part of the northern Luliang arc during the Carboniferous that resulted from the southward subduction of the Keramaili Oceanic basin. The intermediate-acid volcanic rocks in the Shiyintan area display typical I-type granite associations and were most likely generated by the melting of the juvenile basaltic lower crust in a convergent setting. Noteworthy, the western part of the Luliang arc gradually evolved into a mature island arc, as reflected by evidence for an increased crustal component in the melt from the Early Carboniferous (low-K calc-alkali associations in well Y-1) to Late Carboniferous (high-K or shoshonitic associations in well Y-2) (Jakeš and White 1972). During the Early Carboniferous, the oceanic slab moved down with the continuation of subduction, resulting in a higher temperature in the crust-mantle reaction zone. Therefore, increased subducted slab melt was introduced into the magmatic source, as supported by the geochemical evidence from the upper volcanic rocks in well Y-1 (Fig. 14c). During the Late Carboniferous, more mantle-derived magmas metasomatized due to increasing addition of the subducted slab melts to the lower crust, resulting in

the eruption of arc-type high-K and shoshonitic volcanic rocks in well Y-2 (Fig. 14d). The appearance of molasse formations and A-type granitoids around the western Junggar area indicates the end of oceanic plate subduction after the Late Carboniferous (Yin et al. 2011).

It is widely believed that the northern Junggar area experienced a major sequence of subduction–accretion–collision and developed extensive volcano-related rocks during the Late Paleozoic, resulting from the amalgamation of multiple plates (Xu et al. 2012; Zhang et al. 2011, 2017). The Carboniferous is the critical epoch for the evolution of the Keramaili Oceanic basin and collision occurred between the Wulungu arc and the Luliang arc until the post-Carboniferous (Long et al. 2006; Li et al. 2016). The northern part of the Luliang Uplift records the southward subduction of the Keramaili Oceanic basin during the Carboniferous; however, the compositions of the associated volcanic rocks display significant spatial variation (Hui et al. 2009; Su et al. 2010; Zhang et al. 2018). Our data and previous studies both indicate a significant tectonic transition from convergence to extension between the eastern and the western parts of the Luliang Uplift (Li et al. 2012; Han et al. 2019b). Nevertheless, the new results in this study demonstrate that this tectonic difference may

have developed earlier than the Late Carboniferous. According to the eruption ages of the volcanic rocks mentioned above, it was inferred herein that the closure of the Keramaili Oceanic basin in the western part of the northern Luliang arc lagged behind that in the east by at least 34 Ma. The earliest within-plate basalt in the east occurred in the age of 337.2 ± 4.1 Ma (Li et al. 2015a) and the latest arc volcanic rocks in the west appeared in the ages of 303 ± 7.7 Ma (Han et al. 2019a). This tectonic difference existed between the eastern and the western parts of the northern Luliang arc until the emplacement of bimodal volcanic rocks and A-type granite in the western Junggar Basin at the end of the Late Carboniferous, which indicates the existence of a within-plate rift environment (Liu et al. 2016; Yang et al. 2014c; Zhou et al. 2008). Therefore, the Later Carboniferous subduction-related arc-type low-K calc-alkali andesite–dacite assemblages in well Y-1 and the Early Carboniferous bimodal volcanic rocks from outcrop WW' bring the time of formation of this tectonic difference forward to the Early Carboniferous.

7 Conclusions

- Carboniferous low-K to high-K calc-alkali andesite–dacite assemblages occur in the western part of the northern Luliang Uplift, whereas Lower Carboniferous bimodal volcanic rocks are preserved in its eastern part. Although arc-type volcanic rocks are distributed in wells Y-1 and Y-2, the geopolarity of the island arc between these two wells indicated that the formation age of volcanic rocks in well Y-1 was earlier than those in well Y-2.
- The Carboniferous volcanic rocks in well Y-1 show the arc-related magmatic signal, but the upper volcanic rocks consist of more additions from slab melting. Moreover, the limited occurrence of quartz, more mafic minerals, higher REEs, and HSFs concentrations in the upper volcanic rocks in well Y-1 indicate a stronger partial melting of lower continental crust. The binary feature of volcanic rocks in well Y-1 indicates an evolutionary subduction-related magmatic activity in the western part of northern Luliang Uplift during the Early Carboniferous.
- In outcrop WW', the basalts were obtained as the product of the melting of lithospheric mantle that was contaminated by crustal materials during magma upwelling, and their symbiotic dacite–rhyolite associations were derived from partial crustal melting due to underplating. The intermediate-acid volcanic rocks in wells Y-1 and Y-2, with typical arc volcanic rock characteristics, originated from arc-type calc-alkali basaltic magma in the juvenile lower crust. These results indicate a significantly different petrogenesis and magmatism between the eastern and the western parts of the northern Luliang Uplift.
- Opposing geodynamic settings co-existed in the northern Luliang arc during the Carboniferous. The western part of the northern Luliang arc was in a continental marginal environment during the Carboniferous, whereas its eastern part was in an intra-arc extensional setting during the Early Carboniferous. The eastern part of the Keramaili Oceanic basin had been closed before the Early Carboniferous. This tectono-magmatic difference between the eastern and the western parts of the north Luliang Uplift appeared before the Carboniferous period.

Acknowledgements We thank Dr. Zhuangfu Li and Mr. Peiming Zhou for their assistance in lithological analyses. We would also like to extend my gratitude to the two anonymous reviewers for their valuable comments. This research was financially supported by the National Natural Science Foundation of China (Nos. 41802182 and 42072192), Open fund of Key Laboratory of Coalbed Methane Resources and Reservoir Formation Process of the Ministry of Education, China University of Mining and Technology (No. 2018-004), A Project Funded by the Priority Academic Program Development of Jiangsu Higher Education Institution (PAPD) and China Scholarship Council.

References

- Aldanmaz E, Pearce JA, Thirlwall MF, Mitchell JG (2000) Petrogenetic evolution of late Cenozoic, post-collision volcanism in western Anatolia, Turkey. *J Volcanol Geoth Res* 102(1–2):67–95
- Bolge LL, Carr MJ, Feigenson MD, Alvarado GE (2006) Geochemical stratigraphy and magmatic evolution at Arenal Volcano, Costa Rica. *J Volcanol Geoth Res* 157(1):34–48
- Brewer TS, Åhäll KI, Menuge JF, Storey CD, Parrish RR (2004) Mesoproterozoic bimodal volcanism in SW Norway, evidence for recurring pre-Sveconorwegian continental margin tectonism. *Precambr Res* 134(3–4):249–273
- Chen J, Han B, Ji J, Zhang L, Xu Z, He G, Wang T (2010) Zircon U–Pb ages and tectonic implications of Paleozoic plutons in northern West Junggar, North Xinjiang. *China Lithos* 115(1–4):137–152
- Cheng T, Nebel O, Sossi P, Chen F (2015) Assessment of hafnium and iron isotope compositions of Chinese national igneous rock standard materials GSR-1 (granite), GSR-2 (andesite), and GSR-3 (basalt). *Int J Mass Spectrom* 386(1):61–66
- Condie KC (1989) Geochemical changes in basalts and andesites across the Archean-Proterozoic boundary: identification and significance. *Lithos* 23(1):1–18
- Condie KC (2005) High field strength element ratios in Archean basalts: a window to evolving sources of mantle plumes? *Lithos* 79(3–4):491–504
- Defant MJ (1992) The geochemistry of young volcanism throughout western Panama and southeastern Costa Rica: an overview. *J Geol Soc* 149(4):569–579
- Defant MJ, Drummond MS (1990) Derivation of some modern arc magmas by melting of young subducted lithosphere. *Nature* 347(6294):662

- Eby, and Nelson, G. (1992) Chemical subdivision of the a-type granitoids: petrogenetic and tectonic implications. *Geology* 20(7):641
- Ewart A (1982) The mineralogy and petrology of Tertiary-Recent orogenic volcanic rocks with special reference to the andesite-basaltic compositional range. In: Thorpe RS (ed) *Andesites*. John Wiley and sons, New York, pp 25–95
- Fitton JG, James D, Kempton PD, Ormerod DS, Leeman WP (1988) The role of lithospheric mantle in the generation of late Cenozoic basic magmas in the western United States. *J Petrol* 29(1):331–349
- Frey FA, Green DH, Roy SD (1978) Integrated models of basalt petrogenesis: a study of quartz tholeiites to olivine melilitites from southeastern Australia utilizing geochemical and experimental petrological data. *J Petrol* 19:463–513
- Garrison JM, Davidson JP (2003) Dubious case for slab melting in the Northern volcanic zone of the Andes. *Geology* 31(6):565–568
- Genç ŞC, Tüysüz O (2010) Tectonic setting of the Jurassic bimodal magmatism in the Sakarya Zone (Central and Western Pontides, Northern Turkey: a geochemical and isotopic approach. *Lithos* 118(1–2):95–111
- Geng H, Min S, Chao Y, Xiao W, Xian W, Zhao G, Zhang L, Wong K, Wu F (2009) Geochemical, Sr-Nd and zircon U-Pb-Hf isotopic studies of late Carboniferous magmatism in the West Junggar, Xinjiang: implications for ridge subduction? *Chem Geol* 266(3–4):364–389
- Geng H, Sun M, Yuan C, Zhao G, Xiao W (2011) Geochemical and geochronological study of Early Carboniferous volcanic rocks from the west Junggar: petrogenesis and tectonic implications. *J Asian Earth Sci* 42(5):854–866
- Gladney ES, Jones EA, Nickell EJ, Roelandts I (1992) 1988 compilation of elemental concentration data for USGS AGV-1, GSP-1, and G-2. *Geostand Geoanal Res* 16(2):111–300
- Gorton MP, Schandl ES (2000) From continents to island arcs: a geochemical index of tectonic setting for arc-related and within-plate felsic to intermediate volcanic rocks. *The Canadian Mineralogist* 38(5):1065–1073
- Gou J, Sun D, Liu Y, Ren Y, Zhao Z, Liu X (2013) Geochronology, petrogenesis, and tectonic setting of Mesozoic volcanic rocks, southern Manzhouli area. *Inner Mongolia Int Geol Rev* 55(8):1029–1048
- Grove TL, Elkins-Tanton LT, Parman SW, Chatterjee N, Müntener O, Gaetani GA (2003) Fractional crystallization and mantle-melting controls on calc-alkaline differentiation trends. *Contrib Miner Petrol* 145(5):515–533
- Han B, Ji J, Song B, Chen L, Zhang L (2006) Late Paleozoic vertical growth of continental crust around the Junggar Basin, Xinjiang, China (part I): timing of postcollisional plutonism. *Acta Petrologica Sinica* 22(5):1077–1086
- Han S, Sang S, Wang W, Li Z, Liu W, Zhang K (2015) Geochemical characteristics and tectonic setting of Lower Carboniferous volcanic rocks from Wunan-Ludong area, Junggar basin. *China Himal Geol* 36(2):118–125
- Han S, Sang S, Liang J, Wang W, Zhang G, Wang S (2019a) Geochemistry, petrology, and U-Pb dating of high-K volcanic rocks in wells WC-1 and Y-2 from the northern Junggar Basin, northwestern China: implications for the closure of the Karamaili oceanic basin during the Carboniferous. *Geol J* 54:3921–3939
- Han S, Sang S, Liang J, Wang W, Zhang G, Wang S (2019b) Characteristics and genesis of diachronous Carboniferous volcano-sedimentary sequences: insights from geochemistry, petrology and U-Pb dating in the north Junggar basin. *China Int Geol Rev* 61(4):404–423
- He G, Liu J, Zhang Y, Xu X (2007) Karamay ophiolitic mélange formed during Early Paleozoic in western Junggar basin. *Acta Petrologica Sinica* 23(7):829–831
- He Y, Zhao G, Sun M, Wilde SA (2008) Geochemistry, isotope systematics and petrogenesis of the volcanic rocks in the Zhongtiao Mountain: an alternative interpretation for the evolution of the southern margin of the North China Craton. *Lithos* 102(1):158–178
- Hui Y, Weng B, Zhang Y, Zhang G, Liu Z, Wu F, Wei Y, Dai X, Hu Q (2009) Distribution of hydrocarbon traps in volcanic rocks and optimization for selecting exploration prospects and targets in Junggar Basin: case study in Ludong-Wucuiwan area. NW China. *Petrol Explor Dev* 36(4):419–427
- Jakeš P, White AJR (1972) Hornblendes from calc-alkaline volcanic rocks of island arcs and continental margins. *American Mineralogist* 57(5–6):887–902
- Kou Y, Shi Y, Li B, Qin X, Wang L, Li X (2010) The complex lithology rock-electricity features of volcanic rocks in Kelameili gas field. *Acta Petrologica Sinica* 26(1):291–301
- La Flèche M, Camiré G, Jenner G (1998) Geochemistry of post-acadian, Carboniferous continental intraplate basalts from the Maritimes Basin, Magdalen islands, Québec. *Canada Chem Geol* 148(3–4):115–136
- Le Maitre RW (1989) A classification of igneous rocks and glossary of terms. Blackwell, Oxford, pp 1–193
- Li D, He D, Tang Y, Fan C, Kong Y (2012) Genesis of Early Carboniferous volcanic rocks of the Di'nan uplift in Junggar Basin: constraints to the closure time of Kalamaili Ocean. *Acta Petrologica Sinica* 28(8):2340–2354
- Li P, Yuan C, Sun M, Long X, Cai K (2014) Thermochronological constraints on the Late Paleozoic tectonic evolution of the southern Chinese Altai. *J Asian Earth Sci* 113:51–60
- Li D, He D, Santosh M, Ma D (2015a) Tectonic framework of the northern Junggar basin part II: the island arc basin system of the western Luliang uplift and its link with the west Junggar terrane. *Gondwana Res* 27(3):1110–1130
- Li D, He D, Santosh M, Ma D, Tang J (2015b) Tectonic framework of the northern Junggar basin part I: the eastern Luliang uplift and its link with the east Junggar terrane. *Gondwana Res* 27(3):1089–1109
- Li D, He D, Tang Y (2016) Reconstructing multiple arc-basin systems in the Altai–Junggar area (NW China): implications for the architecture and evolution of the western Central Asian Orogenic Belt. *J Asian Earth Sci* 121:84–107
- Liang P, Chen H, Han J, Wu C, Zhang WF, Zhao L, Wang Y (2017) The Early Carboniferous tectonic transition in the northern margin of East Junggar: constraints from geochronology and geochemistry of alkali granites. *Geotectonica Et Metallogenia* 41(1):202–221
- Liu G, Zhu Z, She J, Deng H, Zhao T, Wang Q, Sun Y (2016) Geochronology, geochemistry and petrogenesis of the Zhulume A-type granites in west Junggar. *Xinjiang Geol Rev* 62(2):331–342
- Long X, Sun M, Yuan C, Xiao WJ, Chen H, Zhao Y, Cai K, Li J (2006) Genesis of Carboniferous volcanic rocks in the eastern Junggar: constraints on the closure of the Junggar Ocean. *Acta Petrologica Sinica* 22(1):31–40
- Ludden J, Gélinais L, Trudel P (1982) Archean metavolcanics from the Rouyn-Noranda district, Abitibi Greenst. *Can J Earth Sci* 19(12):2276–2287
- Luo T, Liao Q, Zhang X, Chen J, Wang G, Huang X (2016) Geochronology and geochemistry of carboniferous metabasalts in eastern Tianshan, Central Asia: evidence of a back-arc basin. *Int Geol Rev* 58(6):756–772
- Luo T, Liao Q, Chen J, Hu C, Wang F, Chen S, Wu W, Tian J, Fan G (2017) A record of post-collisional transition: evidence from

- geochronology and geochemistry of Palaeozoic volcanic rocks in the eastern Junggar. *Central Asia Int Geol Rev* 59(10):1256–1275
- Mao X (2012) Research on tectonic lithofacies paleogeography and source rocks characteristics of the Carboniferous–Early Permian in the northern part of Junggar Basin (MS thesis). Northwest University, Xi'an, pp 11–13
- Mao Z, Zou C, Zhu R, Guo H, Wang J, Yong T (2010) Geochemical characteristics and tectonic settings of Carboniferous volcanic rocks in Junggar basin. *Acta Petrologica Sinica* 26(1):207–216
- Martin H, Smithies RH, Rapp R, Moyen JF, Champion D (2005) An overview of adakite, tonalite-trondhjemite-granodiorite (TTG), and sanukitoid: relationships and some implications for crustal evolution. *Lithos* 79(1–2):1–24
- Meschede M (1986) A method of discriminating between different types of mid-ocean ridge basalts and continental tholeiites with the Nb–Zr–Y diagram. *Chem Geol* 56(3–4):207–218
- Pearce JA (1982) Trace elements characteristics of lavas from destructive plate boundaries. In: Thorpe RS (ed) *Andesites*. Wiley, New York, pp 525–548
- Pearce JA (1983) Role of the sub-continental lithosphere in magma genesis at active continental margins. *Continental Basalts and Mantle Xenoliths* 147:2162–2173
- Pearce JA (2008) Geochemical fingerprinting of oceanic basalts with applications to ophiolite classification and the search for Archean oceanic crust. *Lithos* 100(1–4):14–48
- Pearce JA, Cann JR (1973) Tectonic setting of basic volcanic rocks determined using trace element analyses. *Earth Planet Sci Lett* 19(2):290–300
- Pearce JA, Mei H (1990) Lasa to Geermu volcanic rocks. In: Team C-B-T, Expedition PGCS (eds) *Qinghai-Tibet Plateau Geological Evolution*. Science Press, Beijing, pp 174–205
- Pearce JA, Norry MJ (1979) Petrogenetic implications of Ti, Zr, Y, and Nb variations in volcanic rocks. *Contrib Miner Petrol* 69(1):33–47
- Pearce JA, Harris NB, Tindle AG (1984) Trace element discrimination diagrams for the tectonic interpretation of granitic rocks. *J Petrol* 25(4):956–983
- Plank T (2005) Constraints from thorium/lanthanum on sediment recycling at subduction zones and the evolution of the continents. *J Petrol* 46(5):921–944
- Şengör AC, Natal'in BA, Sunal G, Rob VDV (2018) The tectonics of the Altaids: crustal growth during the construction of the continental lithosphere of Central Asia between ~750 and ~130 Ma ago. *Annu Rev Earth Planet Sci* 46(1):439–494
- Shellnutt JG, Bhat GM, Wang KL, Brookfield ME, Dostal J, Jahn BM (2012) Origin of the silicic volcanic rocks of the Early Permian Panjal Traps, Kashmir. *India Chem Geol* 334(2):154–170
- Shen P, Pan H, Xiao W, Li X, Dai H, Zhu H (2013) Early Carboniferous intra-oceanic arc and back-arc basin system in the west Junggar. *NW China Int Geol Rev* 55(16):1991–2007
- Su Y, Zheng J, Griffin WL, Tang H, O'Reilly SY, Lin X (2010) Zircon U–Pb and Hf isotopes of volcanic rocks from the Batamayineishan Formation in the eastern Junggar Basin. *Chin Sci Bull* 55(36):4150–4161
- Su B, Qin K, Sakyi P, Li X, Yang Y, Sun H, Tang D, Liu P, Xiao Q, Malaviarachchi SPK (2011) U–Pb ages and Hf–O isotopes of zircons from Late Paleozoic mafic-ultramafic units in southern Central Asian Orogenic Belt: tectonic implications and evidence for an Early-Permian mantle plume. *Gondwana Res* 20(2–3):516–531
- Su Y, Zheng J, Griffin WL, Zhao J, Tang H, Ma Q, Lin X (2012) Geochemistry and geochronology of Carboniferous volcanic rocks in the eastern Junggar terrane, NW China: implication for a tectonic transition. *Gondwana Res* 22(3–4):1009–1029
- Sun SS, McDonough WF (1989) Chemical and Isotopic Systematics of oceanic basalts: implications for Mantle Composition and Processes. *Geol Soc London Spec Publ* 42(1):313–345
- Tan J, Wu R, Zhang Y, Wang S, Guo Z (2009) Characteristics and geochronology of volcanic rocks of Batamayineishan formation in Kalamaili, eastern Junggar. *Xinjiang Acta Petrologica Sinica* 25(3):539–546
- Tang G, Wang Q, Wyman DA, Li Z, Zhao Z, Jia X, Jiang Z (2010) Ridge subduction and crustal growth in the Central Asian Orogenic Belt: evidence from Late Carboniferous adakites and high-Mg diorites in the western Junggar region, northern Xinjiang (west China). *Chem Geol* 277(3–4):281–300
- Tao H, Wang Q, Yang X, Jiang L (2013) Provenance and tectonic setting of late carboniferous clastic rocks in West Junggar, Xinjiang, China: a case from the Hala-alat Mountains. *J Asian Earth Sci* 64:210–222
- Tian W, Campbell IH, Allen CM, Guan P, Pan W, Chen M, Yu H, Zhu W (2010) The Tarim picrite–basalt–rhyolite suite, a Permian flood basalt from northwest China with contrasting rhyolites produced by fractional crystallization and anatexis. *Contrib Miner Petrol* 160(3):407–425
- Walowski KJ, Wallace PJ, Hauri EH, Wada I, Clynnne MA (2015) Slab melting beneath the Cascade Arc driven by dehydration of altered oceanic peridotite. *Nat Geosci* 8(5):404
- Wang F, Yang M, Zheng J (2002) Geochemical characteristics and geological environment of basement volcanic rocks in Luliang, central region in Junggar basin. *Acta Petrologica Sinica* 18(1):9–16
- Whalen JB, Currie KL, Chappell BW (1987) A-type granites: geochemical characteristics, discrimination and petrogenesis. *Contrib Miner Petrol* 95(4):407–419
- Winchester JA, Floyd PA (1977) Geochemical discrimination of different magma series and their differentiation products using immobile elements. *Chem Geol* 20(4):325–343
- Windley BF, Alexeiev D, Xiao W, Kröner A, Badarch G (2007) Tectonic models for accretion of the Central Asian Orogenic Belt. *J Geol Soc* 164(1):31–47
- Wu X, Liu D, Wei G, Li J, Li Z (2009) Geochemical characteristics and tectonic settings of carboniferous volcanic rocks from Ludong–Wucaiwan area. *Junggar basin Acta Petrologica Sinica* 25(1):55–66
- Wu X, Li J, Yang D, Zhang C, Hou L, Zheng M (2011) The electric characteristics and seismic response of Carboniferous volcanic rock in Ludong–Wucaiwan area of Junngar basin. *Chinese J Geophys* 54(2):481–490
- Xia L (2014) The geochemical criteria to distinguish continental basalts from arc related ones. *Earth Sci Rev* 139:195–212
- Xiao W, Windley BF, Yuan C, Sun M, Han C, Lin S, Chen H, Yan Q, Liu D, Qin K, Li J, Sun S (2009) Paleozoic multiple subduction-accretion processes of the southern Altaids. *Am J Sci* 309(3):221–270
- Xiao Y, Zhang H, Shi J, Su B, Sakyi PA, Lu X, Hu Y, Zhang Z (2011) Late Paleozoic magmatic record of East Junggar, NW China and its significance: implication from zircon U–Pb dating and Hf isotope. *Gondwana Res* 20(2–3):532–542
- Xu Z, Han B, Ren R, Zhou Y, Zhang L, Chen J, Su L, L X, D L (2012) Ultramafic–mafic mélange, island arc and post-collisional intrusions in the mayile mountain, west Junggar, China: implications for Paleozoic intra-oceanic subduction-accretion process. *Lithos* 132–133:141–161
- Xu X, Jiang N, Li X, Wu C, Qu X, Zhou G, Dong L (2015) Spatial–temporal framework for the closure of the Junggar Ocean in central Asia: New SIMS zircon U–Pb ages of the ophiolitic mélange and collisional igneous rocks in the Zhifang area, East Junggar. *J Asian Earth Sci* 111:470–491

- Yang F, Chen G (2016) The basement property and evolution of the northern Junggar basin-evidence from zircon U-Pb chronology and trace element. *Arab J Geosci* 9(5):353
- Yang H, Chen L, Kong Y (2004) A novel classification of structural units in Junggar Basin. *Xinjiang Petroleum Geol* 25(6):686–688
- Yang H, Wen B, Zhang Y, Zhang G, Liu Z, Wu F, Wei Y, Dai X, Hu Q (2009) Distribution of hydrocarbon traps in volcanic rocks and optimization for selecting exploration prospects and targets in Junggar Basin: Case study in Ludong-Wucuiwan area. *NW China Pet Explor Dev* 36(4):419–427
- Yang G, Li Y, Li Z, Liu X, Yang B, Wu H (2010) Genesis and tectonic settings of post-collision volcanic rocks in north eastern margin of East Junggar. *Xinjiang Earth Sci Front* 17(1):49–60
- Yang X, He D, Wang Q, Tang Y, Tao H, Li D (2012) Provenance and tectonic setting of the carboniferous sedimentary rocks of the East Junggar basin, China: evidence from geochemistry and U-Pb zircon geochronology. *Gondwana Res* 22(2):567–584
- Yang F, Chen G, Hou B, Zhang J, Hu Y, Huang D (2014a) Zircon U-Pb, trace elements and Hf isotopes of pyroclastic rocks from the drilling cores in the Junggar basin. *Acta Geol Sin* 88(6):1068–1080
- Yang G, Li Y, Safonova I, Yi S, Tong L, Seltnann R (2014b) Early Carboniferous volcanic rocks of west Junggar in the western central asian orogenic belt: implications for a supra-subduction system. *Int Geol Rev* 56(7):823–844
- Yang G, Li Y, Yan J, Tong L, Han X, Wang Y (2014c) Geochronological and geochemical constraints on the origin of the 304 ± 5 ma Karamay A-type granites from west Junggar, northwest China: implications for understanding the Central Asian Orogenic Belt. *Int Geol Rev* 56(4):393–407
- Yang G, Li Y, Tong L, Li G, Wu L, Wang Z (2016) Petrogenesis and tectonic implications of early Carboniferous alkaline volcanic rocks in Karamay region of West Junggar. *Northwest China Int Geol Rev* 58(10):1278–1293
- Yin J, Yuan C, Wang Y, Long X, Guan Y (2011) Magmatic records on the Late Paleozoic tectonic evolution of western Junggar Xinjiang. *Geotectonica et Metallogenia* 35(2):278–291
- Zhang S, Shi X, Kong Y, Shi J, Lei T, Fang L, Sun G (2008a) Geochemical characteristics and tectonic setting of the Permian-Carboniferous volcanic rocks in Luxi area of Junggar basin. *J Mineralogy Petrol* 28(2):71–75
- Zhang Z, Mao J, Cai J, Kusky TM, Zhou G, Yan S, Zhao L (2008b) Geochemistry of picrites and associated lavas of a Devonian island arc in the northern Junggar terrane, Xinjiang (NW China): Implications for petrogenesis, arc mantle sources and tectonic setting. *Lithos* 105(3):379–395
- Zhang J, Xiao W, Han C, Mao Q, Ao S, Guo Q, Ma C (2011) A devonian to Carboniferous intra-oceanic subduction system in western Junggar. *NW China Lithos* 125(1–2):592–606
- Zhang S, Zhu J, Ge W, Liu S, Lu X, Zhang S, Shi J (2015a) Significant of volcanic eruption spatiotemporal sequence in Batamayineishan formation, Ludong region, Junggar basin. *J Central South Univ* 46(1):199–207
- Zhang Y, Guo Z, Pe-Piper G, Piper DJ (2015b) Geochemistry and petrogenesis of Early Carboniferous volcanic rocks in East Junggar, North Xinjiang: Implications for post-collisional magmatism and geodynamic process. *Gondwana Res* 28(4):1466–1481
- Zhang X, Zhao G, Eizenhöfer PR, Sun M, Han Y, Hou W, Liu D, Wang B, Liu Q, Xu B, Zhu CY (2016) Tectonic transition from Late Carboniferous subduction to Early Permian post-collisional extension in the eastern Tianshan, NW China: insights from geochronology and geochemistry of mafic–intermediate intrusions. *Lithos* 256–257:269–281
- Zhang D, Zhou T, Yuan F, White N, Hollings P, Xiao W, Deng Y, Zhao B, Wang JL (2017) Genesis of Late Carboniferous granitoid intrusions in the Dayinsu area, west Junggar, Northwest China: evidence of an arc setting for the western CAO. *Int Geol Rev* 59(9):1–15
- Zhang G, Lin H, Zhang K, Xu W (2018) Petrologic characteristics of carboniferous volcanic rocks in Luxi, Junggar Basin, and their geological significance. *Geol Rev* 64(1):77–90
- Zhao Z, Wang Q, Xiong X (2004) Complex mantle-crust interaction in subduction zone. *Bulletin Mineralogy, Petrol Geochem* 23(4):277–284
- Zheng R, Zhao L, Yang Y (2019) Geochronology, geochemistry and tectonic implications of a new ophiolitic mélange in the northern West Junggar, NW China. *Gondwana Res* 74:237–250
- Zhou T, Yuan F, Fan Y, Zhang D, Cooke D, Zhao G (2008) Granites in the Sawuer region of the west Junggar, Xinjiang Province, China: geochronological and geochemical characteristics and their geodynamic significance. *Lithos* 106(3):191–206
- Zhou Y, Zhu W, Chen Z, Zheng B, Shao X, Xue F (2018) Volcanic rocks distribution and basement structure in western–central Junggar Basin revealed by gravitational and magnetic data. *Geol J* 53(3):960–976